

2007

Development of a field effect transistor using a DNA-biopolymer as the semiconducting layer

Carrie Marie Bartsch
University of Dayton

Follow this and additional works at: https://ecommons.udayton.edu/graduate_theses

Recommended Citation

Bartsch, Carrie Marie, "Development of a field effect transistor using a DNA-biopolymer as the semiconducting layer" (2007). *Graduate Theses and Dissertations*. 1419.
https://ecommons.udayton.edu/graduate_theses/1419

This Dissertation is brought to you for free and open access by the Theses and Dissertations at eCommons. It has been accepted for inclusion in Graduate Theses and Dissertations by an authorized administrator of eCommons. For more information, please contact mschlange1@udayton.edu, ecommons@udayton.edu.

DEVELOPMENT OF A FIELD EFFECT TRANSISTOR
USING A DNA-BIOPOLYMER AS THE
SEMICONDUCTING LAYER

Dissertation

Submitted to

The School of Engineering of the

UNIVERSITY OF DAYTON

In Partial Fulfillment of the Requirements for

The Degree

Doctor of Philosophy in Electrical Engineering

by

Carrie Marie Bartsch

UNIVERSITY OF DAYTON

Dayton, Ohio

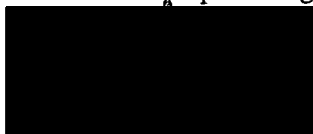
August 2007

DEVELOPMENT OF A FIELD EFFECT TRANSISTOR USING A DNA-BIOPOLYMER
AS THE SEMICONDUCTING LAYER

APPROVED BY:



Guru Subramanyam, Ph.D.
Advisor Committee Chairman
Associate Professor, Department of
Electrical and Computer Engineering



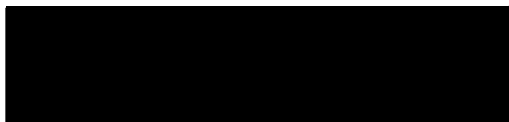
Partha P. Banerjee, Ph.D.
Committee Member
Professor, Department of Electrical and
Computer Engineering



James G. Grote, Ph.D.
Committee Member
Senior Electronics Research Engineer,
Air Force Research Laboratory



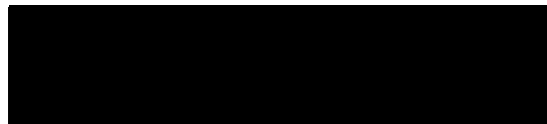
Andrew M. Sarangan, Ph.D.
Committee Member
Associate Professor, Electro-Optics
Program



Gerald Shaughnessy
Committee Member
Associate Professor, Department of
Mathematics



Malcolm W. Daniels, Ph.D.
Associate Dean
School of Engineering



Joseph E. Saliba, Ph.D., P.E.
Dean
School of Engineering

© Copyright by

Carrie Marie Bartsch

All rights reserved

2007

ABSTRACT

DEVELOPMENT OF A FIELD EFFECT TRANSISTOR USING A DNA-BIOPOLYMER AS THE SEMICONDUCTING LAYER

Name: Bartsch, Carrie Marie
University of Dayton

Advisor: Dr. Guru Subramanyam

Research in thin film biopolymers is an exciting area with a wide variety of applications. The advantages of using these thin films in electro-optic and electronic applications in place of organic polymers are being studied. This dissertation focuses on the use of biopolymer materials, particularly deoxyribonucleic acid (DNA), in thin film electronic devices.

DNA-biopolymers are explored for use as the semiconducting material in a field effect transistor using both top gate and bottom gate transistor structures. Strong nonlinear switching behavior is observed in these transistor structures. One of the DNA-biopolymers studied is formed by mixing DNA with poly(3,4-ethylenedioxythiophene) poly(styrenesulfonate) (PEDOT:PSS) and adding excess hexadecyltrimethylammonium chloride (CTMA) into the complex, and is called DNA:PEDOT:CTMA. This DNA-biopolymer is shown to operate as a semiconducting material in these transistors. The effective mobility of DNA:PEDOT:CTMA is determined through analysis of the current-voltage curves produced by the transistor. In the linear region of operation, the mobility is found to be $0.018 \text{ cm}^2/(\text{Vs})$. In the saturation region, the mobility is found to be $0.45 \text{ cm}^2/(\text{Vs})$.

A second device that employs these biopolymer thin films is a new capacitive test structure. This structure contains a parallel plate capacitor with coplanar waveguide feed lines and is used

to obtain the dielectric properties of the thin film contained within the capacitor. The dielectric properties of the biopolymer, specifically the relative dielectric constant and dielectric loss-tangent, are obtained at microwave frequencies as a function of temperature and applied bias. It is found that these properties change with applied bias in the biopolymers. As much as 52% dielectric tuning is observed for capacitive test structures containing thin films of DNA-CTMA.

For Mark

ACKNOWLEDGMENTS

A doctoral dissertation bears only one name even though graduate school and research are collaborative processes. I could not have made it this far without the help and support of many others who deserve my thanks and appreciation!

First, my profound thanks go to my advisors, Dr. Guru Subramanyam and Dr. Jim Grote, for providing me with steady guidance, great opportunities, and never-ending encouragement. I also want to thank the other members of my committee, Dr. Partha Banerjee, Dr. Andrew Sarangan, and Prof. Gerald Shaughnessey, for guiding me to new knowledge and helping me through this process.

I want to thank Dr. Emily Heckman and Dr. Josh Hagen for guiding the start of my path with their own graduate work and answering my never-ending questions. My thanks also go to my collaborators at Wright Patterson's Air Force Research Laboratory: Mrs. Kristi Singh, Mr. Gerry Landis, Mr. Tom Kensky, Capt. Joe Akin, Mr. Steve Smith, Dr. Perry Yaney, Dr. Angela Campbell, Dr. Larry Brott, Mr. Will Mitchell, Dr. Ken Hopkins, Dr. Rajesh Naik, Ms. Sharon Jones, Dr. Bill Mitchel, Mr. Dan Shallenberger, and Mr. Scott Axtell, for insightful discussions, technical assistance, sanity checks, and guiding my research beyond my own area of expertise. I also want to thank Miss Holly Zelnio, Ms. Angela Griffith, Mr. Hans Spaeth, and Dr. Fahima Ouchen for assisting with the processing of the DNA-biopolymers and helping to lighten my load. My special thanks go to Mr. Bob Jones and Dr. Andrew Steckl, at the University of Cincinnati, for helping with the molecular beam deposition of the thin films.

I also want to thank Dr. Birendra Singh and Dr. Serdar Sariciftci, at the Linz Institute of Organic Solar Cells at the Johannes Kepler University of Linz, for laying the groundwork for the DNA-based transistor. My thanks also go to Dr. Naoya Ogata, at the Chitose Institute of Science and Technology (CIST), for making the DNA material available.

I would like to gratefully acknowledge the support of the National Science Foundation (NSF), the Dayton Area Graduate Studies Institute (DAGSI), Air Force Research Laboratory Materials and Manufacturing Directorate (AFRL/ML), and the Defense Advanced Research Projects Agency Defense Sciences Office (DARPA/DSO).

My thanks also go to my graduate advisor at the University of Michigan, Dr. John Whitaker, for guiding my master's degree research and showing me how to combine the fields of optics and microwave circuits in various research projects.

I would be remiss if I didn't also thank my mentor and undergraduate advisor at the University at Buffalo, Dr. Alex Cartwright, who had the foresight to welcome me into his research lab, guide my first research endeavor into the unknown, treat me as though I was just as capable as his senior graduate students, and encourage me to dream big and reach for my dreams even in the face of difficulties!

I also want to thank all my family and friends whose support and faith in my abilities give me the strength to keep moving forward. My thanks go especially to my parents, who have given me not only life but also an unquenchable thirst for knowledge. They always expect me to do my best, and regularly remind me that I am "lovable and capable!" My parents support and encourage my dreams, and they celebrate every success with me! My special thanks go to my siblings, John Edward and Christa, who always believe in my ability to succeed, and to Christa's family (her husband, Jonathan, and her son, Joseph) for providing their love, support, and encouragement. I

would also like to thank all of my grandparents, whose never-ending love and support provide me with the strength to go the distance and never give up, even when the path ahead is rocky. My thanks also go to my mother-in-law and father-in-law who understand the importance of education and never complain when our time with them is scarce, and to my brother-in-law, Michael, who accepts me as his sister and reminds me to enjoy my successes.

Most of all, I want to abundantly thank Mark, my best friend, my husband, and my love, for his unwavering support, never-ending encouragement, loving guidance and insightful proof-reading! I could not complete this without his confidence in my abilities!

TABLE OF CONTENTS

	Page
Abstract	iii
Dedication	v
Acknowledgments	vi
List of Figures	xii
List of Tables	xv
 CHAPTERS:	
I. INTRODUCTION	1
1.1 Motivation	2
1.1.1 Why DNA?	4
1.1.2 Why BSA?	5
1.2 Research Objectives	6
1.3 Contributions	7
1.4 Significance	8
1.5 Structure	9
II. BACKGROUND	11
2.1 Existing polymer dielectric materials	11
2.1.1 BCB	11
2.1.2 Polyimides	12
2.1.3 PVA	13
2.1.4 PMMA	14
2.1.5 Polycarbonate	15
2.2 New polymer dielectric materials	16
2.2.1 DNA-biopolymer	16
2.2.2 BSA-biopolymer	18
2.3 Microwave characterization	18

2.4	Field effect transistors	20
2.4.1	Polymer FETs	21
2.4.2	All-polymer FETs	21
2.4.3	Sensor applications	22
2.5	Summary	23
III.	BIOPOLYMER PROCESSING TECHNIQUES	24
3.1	DNA-based biopolymers	24
3.1.1	DNA-CTMA	24
3.1.2	DNA:PEDOT:CTMA	25
3.2	Agarose Gel Electrophoresis	26
3.3	Thin-film deposition	29
3.3.1	Spin coating	29
3.3.2	Molecular Beam Deposition	31
3.4	Summary	33
IV.	ELECTRICAL CHARACTERIZATION OF BIOPOLYMERS	34
4.1	Capacitive Test Structure	34
4.2	Experimental Procedure	39
4.3	Results and analysis	42
4.3.1	APC	45
4.3.2	PVA	46
4.3.3	BSA-PVA	47
4.3.4	DNA-CTMA	52
4.3.5	BST	56
4.4	Capacitance Measurements	56
4.5	Electric Force Microscopy	59
4.6	Summary	63
V.	DNA-BIOPOLYMER SEMICONDUCTOR DEVICES	65
5.1	Measurement setup	65
5.2	Top Gate BioFET Structure	67
5.2.1	Results with DNA-CTMA	69
5.2.2	Results with DNA:PEDOT:CTMA	70
5.2.3	All-DNA BioFET	72
5.3	Bottom Gate BioFET Structure	74
5.3.1	Results	76
5.3.2	Analysis	80

5.4 Summary	83
VI. CONCLUSIONS AND FUTURE WORK	85
6.1 Contributions	85
6.2 Future Work	87
Bibliography	90
Vita	99

LIST OF FIGURES

<u>Figure</u>	<u>Page</u>
3.1 The 1 Kbp DNA ladder, as seen in standard literature.	28
3.2 Results of an agarose gel electrophoresis run with the determined molecular weight values superimposed on top.	29
4.1 A three dimensional representation of the capacitive test structure, showing the overlap of the signal conductor in the top-metal and the shunt line in the bottom metal which form the test capacitor. Notice that the large ground pad capacitor is in series with the test capacitor, resulting in the equivalent capacitance of the test capacitor. .	36
4.2 A photograph of a capacitive test structure with the CPW probes in place to make microwave measurements.	37
4.3 The electrical model for the capacitive test structure.	37
4.4 The microwave probe station pictured with the right probe on a capacitive test structure containing BSA-PVA and the left probe hovering above the sample.	40
4.5 An example of the AWR Microwave Office screen while matching circuit parameters with the measured S parameters. The graphs of S11 and S12 with both experimental and theoretical data from the model are seen on the left side of this figure. The electrical model and the variable tuner are seen on the right side of this figure.	41
4.6 The frequency response of S21 for a capacitive test structure of APC.	45
4.7 The frequency response of S21 for a capacitive test structure containing PVA. . . .	46
4.8 The frequency response of S21 for a capacitive test structure containing BSA-PVA for various applied biases from 0 to 20 V.	47

4.9	The calculated relative dielectric constant as a function of applied voltage for BSA-PVA using the measured S parameters from a capacitive test structure at room temperature.	48
4.10	The frequency response of S21 for a capacitive test structure containing BSA-PVA at 100 C for various applied biases from 0 to 20 V.	50
4.11	The calculated relative dielectric constant as a function of applied voltage for BSA-PVA using the measured S parameters from a capacitive test structure at 100 C. . .	50
4.12	The frequency response of S21 for a capacitive test structure containing DNA-CTMA at room temperature for various applied biases from 0 to 20 V.	53
4.13	The calculated relative dielectric constant as a function of applied voltage for DNA-CTMA using the measured S parameters from a capacitive test structure.	54
4.14	The frequency response of S21 for a capacitive test structure containing DNA-CTMA at 100 C for various applied biases from 0 to 20 V.	55
4.15	The frequency response of S21 for a capacitive test structure containing BST for applied biases from 0 to 3 V.	57
4.16	Capacitance as a function of frequency on a log scale for one capacitive test structure made with a DNA-CTMA thin film.	58
4.17	TappingMode Topography (left), Electric Force Microscopy (center) and Phase Images (right) with DC biases of (a) 5.5 V and (b) 6.0 V applied to the AFM tip. The phase component of the Electric Field is observed over a 5 micron x 5 micron region in the center of the image.	61
4.18	TappingMode Topography (left), Electric Force Microscopy (center) and Phase Images (right) with DC biases of (a) 6.5 V, (b) 7.0 V and (c) 7.5 V applied to the AFM tip. The phase component of the Electric Field is observed over a 5 micron x 5 micron region in the center of the image.	62
5.1	The probe station setup used for measuring the DNA-based transistors.	66
5.2	A cross-sectional view of the top-gate BioFET containing a DNA-biopolymer in the semiconducting layer.	68

5.3	A photograph of one of the top gate BioFETs containing a DNA-biopolymer as the semiconducting layer.	68
5.4	A set of current-voltage curves obtained from a transistor with DNA-CTMA used as the semiconducting layer.	69
5.5	Current-voltage curves obtained from a transistor with DNA:PEDOT:CTMA used as the semiconducting layer.	71
5.6	Current-voltage curves obtained from the all-DNA BioFET with current compliance set at (a) 100 nA and (b) 200 nA.	73
5.7	A cross-section of the bottom gate BioFET structure.	75
5.8	Drain current as a function of drain voltage as measured on a bottom gate BioFET fabricated on an undoped silicon wafer with a very thin silicon dioxide layer as the gate insulator, clearly showing control by the gate voltage.	76
5.9	Drain current as a function of drain voltage as measured on a bottom gate BioFET on an undoped silicon wafer with an RF sputtered silicon dioxide layer as the gate dielectric.	78
5.10	(a) Drain current as a function of drain voltage as measured on a bottom gate BioFET on an undoped silicon wafer with a very thin silicon dioxide layer as the gate insulator. (b) Gate, drain and source current is plotted as a function of drain voltage for this device, verifying that the gate current is substantially lower than either the source or drain currents. Note that positive current is current leaving the terminal.	79
5.11	Saturation mobility as a function of drain voltage as calculated from the drain current vs. drain voltage data on a bottom gate BioFET with a very thin layer of native silicon dioxide as the gate insulator. The data for this plot is calculated using the drain currents associated with gate voltages of 0 and -10 V, when the drain voltage is 0.2 V, obtained from Figure 5.10.	83

LIST OF TABLES

<u>Table</u>	<u>Page</u>
3.1 Parameters used to obtain APC films from APC dissolved in cyclopentanone	32
3.2 DNA-CTMA thin films from DNA-CTMA dissolved in butanol made from 300 kDa DNA	32
3.3 DNA-CTMA thin films from DNA-CTMA dissolved in butanol made from 1000 kDa DNA	32
4.1 The mean microwave dielectric properties calculated from the S parameter mea- surements for APC, PVA, BSA-PVA, and 1000 kDa DNA-CTMA.	43

CHAPTER I

INTRODUCTION

Thin film biopolymers are interesting materials that have significant promise for a variety of applications. A polymer is a molecule made up of many repeating units [1]. Polymers are both naturally occurring and synthetic materials. These molecules can be arranged into thin films which are flexible materials with many uses. Biopolymers are biologically-based polymers and they can be composed of materials that are not typically used as thin film polymers, such as proteins and deoxyribonucleic acid (DNA). Often, biopolymers have nonlinear optical and dielectric properties. While many polymers have been characterized and are currently being used in electrical devices, biopolymers are comparatively new materials and only a few reports of their use exist.

A few of the reported polymer applications include the use of benzocyclobutene (BCB) as a passivation layer in integrated circuits [2, 3] and inductors [4], polyimides as an insulating material in electronics [5, 6, 7], and poly(methyl methacrylate) (PMMA) as the gate dielectric layer in thin-film transistors [8]. Polymers are also being used in microelectronics where the micro- and nanoscale device sizes have created a need for low relative dielectric constant materials to be used in multilevel interconnect applications [9]. A few reported examples of microelectronic applications include using polyimides as the insulator in metal-insulator-semiconductor (MIS) capacitors [10] and polycarbonates to fabricate microchannels [11].

Biopolymers have shown promise for use in electronic and electro-optic devices. These devices include all-DNA waveguides [12], DNA-based light emitting diodes (LEDs) [13, 14], and biopolymer organic field effect transistors (BioFETs) with a DNA-biopolymer as the gate dielectric material [15, 16]. These applications highlight the potential for the use of biopolymers in electronic and electro-optic devices. Biopolymers are still relatively new materials that need to be thoroughly characterized and studied to determine where they can most successfully be used to improve existing electrical and electro-optic devices.

The properties of biopolymers need to be determined over a wide frequency range and under varying temperature and voltage bias conditions to compare them with the inorganic and organic dielectric thin films that are currently used in electronic applications. Preliminary studies of some of the new biopolymers show that their properties can change with either applied voltage or temperature, which suggests that they might be useful in such applications as sensors and antennas. The properties of biopolymers can be varied by changing the molecular weight or combining the biopolymer with other materials such as crosslinkers, chromophores, metals, rare earth metals, and other polymers. This means that the original properties of a biopolymer are not necessarily the only properties that materials containing that particular biopolymer can have, and in some cases the properties can be changed to meet a desired need by combining the biopolymer with other materials. The effect of these changes on the electro-optic properties of biopolymers has been studied, but how they affect the electrical characteristics of biopolymers is unknown.

1.1 Motivation

Biopolymers are materials of interest for many reasons. They are inexpensive to obtain, easily processed from the raw materials into thin films, and abundantly available. Biopolymers can be

readily doped at high levels with other materials, and this doping has been found to change the electrical properties of the biopolymer, specifically the resistivity, mobility, and relative dielectric constant. These materials are compatible with both organic and inorganic materials and can therefore be mixed with a large variety of materials to change the properties of the biopolymers.

Early studies indicate that the biopolymers investigated in this dissertation have some very interesting properties. For instance, some of the biopolymer thin films have higher relative dielectric constants, lower leakage currents, and lower losses than standard optical thin film polymers, as is shown in Section 4.3. In particular, some of the biopolymers studied appear to have dielectric properties that vary with applied bias or temperature.

Studying the microwave characteristics and electrical properties of dielectric thin films over a wide frequency range indirectly led to the development of a field effect transistor that uses a DNA-biopolymer as the semiconducting layer. Based on the results of the characterization studies and the interest in new semiconducting materials, this dissertation focuses on the development of a field effect transistor that uses a DNA-biopolymer as the semiconducting layer. This is possible because of the ability to successfully mix a variety of materials with the DNA-biopolymer. In the DNA-biopolymer semiconductor, a high conductivity polymer is mixed with the DNA to make a new DNA-biopolymer that has a higher conductivity than DNA-CTMA. The processing techniques used to fabricate field effect transistors with a DNA-biopolymer semiconducting layer are easily integrated into existing device fabrication laboratories. These transistors are also easier to process than silicon-based transistors, and therefore this is an exciting new development for semiconductor technologies.

1.1.1 Why DNA?

In Hokkaido, Japan, over 200,000 tons of salmon are harvested each year, which contains 65,000 tons of sperm as a waste product [17]. Contained in the 65,000 tons of salmon sperm is up to 1500 tons of DNA that can be extracted from the salmon roe and milt sacs as a green material for other uses. The Chitose Institute of Science and Technology (CIST), with support from the Air Force Office of Scientific Research Asian Office of Aerospace Research and Development, have developed a large scale process for DNA extraction and purification. This process involves degrading and eliminating the majority of the proteins through homogenization, enzymatic treatment, and pH control. Then, the material is decolorized through a carbon treatment. Next, it is filtered and acetone is added to precipitate out the purified DNA. Finally, this DNA is freeze-dried [17]. This creates a large, inexpensive resource of purified DNA that is obtained without the use of fossil fuels and is therefore a green material.

DNA is a type of nucleic acid, which means that it is a polymer made up of nucleotide building blocks [1]. DNA nucleotides are base-sugar-phosphate compounds. The general structure of the DNA nucleotides is an organic base, adenine, guanine, cytosine, or thymine, linked to carbon 1 of 2-deoxy- β -D-ribose (a 5 carbon sugar), which is in turn linked to a phosphate group at carbon 5 [1]. DNA is made up of two strands of repeating subunits of nucleotides which are bonded together with strong hydrogen bonds forming through the complementary bases (adenine with thymine and guanine with cytosine). The two strands coil around each other in the well-known double-helix with the complementary bases bonding together along the entire length of the strands [1].

The double-helical structure of DNA yields unique charge transport mechanisms. Within a double stranded DNA molecule, transport occurs through a combination of thermally activated

hole-hopping and standard molecular wire transport mechanisms [18]. Early studies on DNA-biopolymers show that the naturally occurring double-helix remains intact in thin films and the chirality of the double-helix also produces unique properties in the thin films, such as increased electro-optic activity [19]. Therefore, the unique charge transport mechanisms reported in DNA are likely to carry over into the DNA-biopolymers and produce interesting electrical characteristics in the DNA-biopolymers. Finally, these DNA-biopolymers have been made into optically transparent thin films, which are used in electro-optic applications such as light-emitting diodes [14] and optical waveguides [20].

1.1.2 Why BSA?

Bovine serum albumin, or BSA, is a globular protein found in cow's blood. A globular protein is made up of long coils folded into compact, spherical shapes [1]. Most globular proteins are water soluble because they have hydrophilic surfaces that bind with water molecules. The characteristic coiling produces unique surface features including charged areas [1].

BSA belongs to a group of proteins known as serum albumins, which are the most abundant proteins in blood plasma [21]. Serum albumins are made of chains of amino acids that are combined by α helix turns and bridges. BSA is made up of 607 amino acids, with 17 covalent bonds and one free cysteine group [22]. The structure of BSA and its physicochemical properties are well characterized, and BSA is known to be water soluble due to the large number of amino acids from which it is made [22].

The structure of biological systems, including biopolymers of all types, is important and changes can occur due to various forms of energy input. Some effects of optical activity in BSA, including the temperature dependence of both optical rotation and light transmission, are known and reported

[23]. The fluorescence response of BSA bound to various small molecules provides information about the location of binding sites in the BSA [21]. Therefore, studying the electrical properties of BSA as a function of temperature and bias voltage is a natural progression towards increasing the body of knowledge about this globular protein.

1.2 Research Objectives

The primary objective of this dissertation is to show that a DNA-biopolymer can be successfully used as a semiconducting material in a thin film field effect transistor. This will be achieved through the fabrication and testing of various transistor structures. Several DNA-biopolymers will be used as the semiconducting layer in these transistors. Various gate insulators will also be used in developing a successful field effect transistor.

The second objective of this dissertation is the characterization of novel dielectric biopolymer thin films. A new capacitive test structure will be used for microwave characterization of these biopolymers over a wide frequency range and with various bias voltages applied. The dielectric properties of the biopolymers will be compared to those of well-established dielectric polymers. Additional studies, including capacitance measurements as a function of frequency and electric force microscopy, will be performed on the DNA-biopolymer to confirm the results obtained from the microwave characterization study.

The third objective is to define the steps and procedures necessary to fabricate the thin film devices in this dissertation. These steps and procedures include making DNA-biopolymers from the raw materials, analyzing the molecular weight of the DNA, and defining the spin parameters necessary to obtain thin films of specific thicknesses. The spin parameters will be defined for all the polymer thin films used, not just the DNA-biopolymers.

1.3 Contributions

This dissertation contains a number of unique contributions that further the existing knowledge of electrical devices and biopolymers. First, spin coating parameters and techniques necessary to obtain uniform thin films from both standard polymers and the new DNA-biopolymers are determined and presented in this dissertation. Also, the techniques used on standard polymers are compared to those necessary for the new DNA-biopolymers.

Next, this dissertation describes the fabrication and use of a *new* capacitive test structure. This capacitive test structure is used to determine the dielectric properties of the thin film material as a function of frequency, applied bias, and temperature. The dielectric properties are determined for the DNA-based and BSA-based biopolymers, along with a reference polymer, amorphous polycarbonate (APC). All of these materials are compared to a known ferroelectric material, barium strontium titanate (BST). The biopolymers, without any optimization, are seen to have dielectric tunability that is comparable to the ferroelectric material.

The most important contribution of this dissertation is the successful development of the *first* field effect transistor (FET) to contain a DNA-biopolymer as the semiconducting layer. DNA is successfully doped with a conducting polymer to produce the *first* DNA-biopolymer to be used as a semiconducting material. Two different field effect transistor structures are designed, developed, and tested, and two types of DNA-biopolymers are used in the semiconducting layer. The effective saturation mobility of the successful FET is determined to be two orders of magnitude less than the mobility of the conducting polymer. Additionally, the *first* all-DNA bioFET is also designed, fabricated and tested.

1.4 Significance

This dissertation focuses on the use of biopolymer thin films in electrical devices. While these biopolymers are new materials, they have already been used in some applications, but many new applications have yet to be discovered. To help identify applications where these biopolymers will be successful, the materials and their properties need to be studied.

For the first time, biopolymer thin films are characterized using electrical and microwave-frequency characterization studies over a wide frequency range, at a variety of bias voltages, and at various temperatures. Additionally, these studies introduce a new capacitive test structure for characterizing polymers [24]. The biopolymers are characterized using this new capacitive test structure that consists of two metal layers of a unique design that are separated by the polymer thin film of interest. An electrical model for this capacitive test structure converts the measured scattering parameters (S parameters) of the capacitive test structure to the dielectric properties of the thin film. Capacitance is also measured as a function of frequency on one of the biopolymers to verify the results obtained from the microwave characterization measurements.

The DNA-biopolymer transistor in this dissertation represents the first successful use of a DNA-biopolymer as the semiconducting layer to be reported in the open literature. The studies on the field effect transistor with a DNA-biopolymer as the semiconducting layer involve the use of several transistor structures and different DNA-biopolymers. In addition to presenting the transistor structures, the device parameters are determined from the measured data.

1.5 Structure

The layout of the remainder of this dissertation is as follows. Chapter II presents the existing work that relates to this dissertation. It describes various thin-film polymers, their known properties, and some applications of polymers. It also describes some of the new biopolymers based on DNA and BSA and existing, published applications which use these materials.

Chapter III describes the processing techniques used with the new biopolymers. The experimental procedures for creating thin films from the raw materials are discussed. This chapter first explains the processing of the DNA-biopolymers in depth. Then, the gel electrophoresis process, which is used to determine the molecular weight of the DNA, is described. The analysis used to extract the information about the molecular weight from the image produced by gel electrophoresis is also presented. Finally, this chapter examines the thin film deposition methods used in this research, some of the problems encountered, and their solutions.

Chapter IV contains the electrical characterization work performed for this dissertation. This chapter begins with a description of the new capacitive test structure that is used to obtain the dielectric properties of the polymer thin films. Then, an electrical model for the capacitive test structure is presented along with derivations for obtaining the S parameters, relative dielectric constant, and loss tangent. Third, the experimental procedure used to measure the S parameters is described. Fourth, the results obtained by using the described procedure on both polymer and biopolymer films are given and analyzed. Then, low frequency capacitance values are measured and the results are shown. Finally, electric force microscopy measurements are described, the images obtained are presented, and the results are analyzed.

Chapter V describes the development of a field effect transistor using a DNA-biopolymer as the semiconducting layer. This chapter begins with a description of the measurement system used on the transistors studied in this dissertation. Then, a top gate transistor structure that is fabricated in this research is described. Third, the results measured from this device are presented and problems are described. Fourth, the bottom gate transistor structure that is fabricated is described. Finally, the measured results are presented and analyzed.

Chapter VI concludes this dissertation with a summary of the results in this dissertation and presents suggestions for future work on biopolymer electronics.

CHAPTER II

BACKGROUND

Many polymers have previously been studied for use as dielectrics and semiconductors, and new polymers are continually being developed and investigated. Similarly, some techniques for microwave characterization are in place and being used, while other, new techniques are actively being developed and tested. The focus of this dissertation is on determining the electrical and microwave characteristics of polymers; comparing existing, well studied polymers to newer ones; and designing and testing biopolymer-based transistors. Before branching out into this new work, a review of the literature in these areas is presented.

2.1 Existing polymer dielectric materials

Some polymer dielectric materials that have already been thoroughly studied include benzocyclobutene, polyimide, polyvinyl alcohol, poly(methyl methacrylate), polycarbonate and amorphous polycarbonate. This section reviews the existing literature on these dielectric polymers and mentions some of their uses.

2.1.1 BCB

Benzocyclobutene is commonly known as BCB. This photosensitive polymer has a high electrical resistivity [25], high mechanical strength, and excellent optical transparency [26]. BCB has

a low relative dielectric constant of 2.7 and a low loss tangent of 0.0008 at one megahertz. It has a curing temperature of 250 °C and a breakdown voltage of 3×10^6 V/cm [27]. It is thermally stable, suitable for micro-electro-mechanical systems (MEMS) processing at low temperatures, and its bonding strength decreases with increased annealing temperatures [28]. Spin-coating can produce BCB waveguide layers that are useful for prism coupling measurements [29].

BCB can be mixed with most organic solvents and water-based acids [26]. It also adheres well to silicon wafers which makes it useful in silicon-based integrated devices. BCB is typically used as a passivation layer for silicon-based integrated circuits [2] to provide mechanical and environmental protection and to provide stress relief between the packaging and the integrated circuit [3]. BCB is also used as a dielectric layer for silicon and copper based inductors [4] and as an adhesive layer for radio frequency MEMS devices [30]. Lee *et al.* discuss the etching of BCB during the formation of MEMS spiral inductors [31]. BCB is also used in wafer bonding to fabricate three dimensional microfluidic circuits [26, 31].

2.1.2 Polyimides

Polyimides are commonly used as insulating materials in electronics [6]. Polyimide has good mechanical properties, low moisture absorption, a low relative dielectric constant, and a high dielectric breakdown voltage [10, 32, 33]. The shrinking dimensions of microelectronics produce a need for dielectric materials with low relative dielectric constants [9]; this need is often filled by low relative dielectric constant polyimides [10]. Low dielectric polymers are also preferred for the insulating materials of small, high speed devices [33]. Thin-film polyimides are also used in microelectronics and are formed by spin-coating [10]. While polyimides have low relative dielectric constants, decreasing the relative dielectric constant even further will enhance the usefulness of

these polymers. Park *et al.* show that the relative dielectric constant of polyimides can be reduced by fluorination. The relative dielectric constant decreases as the fluorine content increases [33].

The high curing temperature of polyimides often prevents their successful usage in polymer-based electronics. Polyimides can be cross-linked, which decreases the curing temperature to 180 – 200 °C [6, 7] and thereby increases their performance in polymer-based electronics [6]. Cross-linking restricts the orientation of the dipoles thereby reducing the relative dielectric constant [32] and providing stable and reliable electronic performance [6].

The polyimide properties are measured through the use of electronic devices, and the literature also shows that they are used in electronic applications. Metal-polyimide-silicon structures are fabricated by spin-coating to determine the polyimide's dielectric properties [9]. Darwish *et al.* present the use of polyimides as a dielectric within embedded transmission lines [34]. Polyimides are also used in thin-film transistors with silicon dioxide as a dual layer gate insulator [5]. The leakage current and capacitance-frequency characteristics are determined for organic transistors using polyimides as a gate dielectric layer [6]. Unni *et al.* report that cross-linked polyimide gate dielectric layers for pentacene based organic field effect transistors (OFETs) yield the same performance as OFETs with uncrosslinked polyimide gate dielectric layers [7].

2.1.3 PVA

For polyvinyl alcohol (PVA), the relative dielectric constant is shown to be dependent on both temperature and frequency. It is also water soluble [35]. However, the solubility conditions of PVA vary based on the type of PVA, and some types only dissolve in boiling water. The dielectric properties of various PVA mixtures are examined in the literature. Subba Reddy *et al.* consider the blend of polyvinyl pyrrolidone (PVP) and PVA. The relative dielectric constant is found to decrease

with increasing temperature [36]. The blend of conductive polypyrrole with PVA containing ferric chloride has conduction properties that can be varied by adjusting the preparation procedure [37, 38]. This blend yields varied electrical characteristics depending on the direction in which the measurement is taken. Along the longitudinal surface it takes less time for free charges to dominate than it does in the transverse direction [38]. Silver-PVA nano-composite films are found to have electrical resistivities that depend on the amount of silver present in the composite and a breakdown field that is double that of PVA [39]. Doping PVA with ammonium metavanadate causes the glass transition temperature to decrease and the peaks in relative dielectric constant to occur at lower temperatures [40]. The suspension of carbon black in PVA with the addition of a biomolecule increases the thermal and chemical sensitivity of the complex, and therefore this addition improves the performance of thermal and chemical sensors [41].

2.1.4 PMMA

The exact chemical composition of poly(methyl methacrylate) (PMMA) varies by supplier [42]. Solvents for PMMA mentioned in the literature include chloroform, acetone, toluene, and tetrahydrofuran [43]. The relaxation properties and loss tangent of PMMA are both dependent upon the solvent in which the PMMA film is cast [44]. The frequency of the dielectric loss peak is found to decrease as the sample temperature decreases [42]. The refractive index of PMMA increases with increasing force applied to the film [29]. The electrical strength of PMMA, which is the amount of voltage that can be applied to PMMA without failure, gradually increases with increasing frequency [45]. The breakdown strength of PMMA films decrease with temperature at all frequencies, decrease with increasing frequency below the glass transition temperature, and increase with increasing frequency above the glass transition temperature [45].

In the literature, PMMA is used as a gate dielectric. It is a suitable dielectric for flexible thin-film transistors because PMMA has a high electrical resistivity, a relative dielectric constant near that of silicon, and is mechanically stable [8]. The literature also describes measurements made on doped PMMA and PMMA blends. The dielectric properties of doped PMMA are reported by Svorcik *et al.* [46]. The glass transition temperature is an inverse function of the dopant concentration for diphenyl sulfoxide-doped PMMA [46]. Mijovic *et al.* report on the blend of PMMA with Poly(vinylidene fluoride) and concludes that the higher the PMMA content, the higher the frequency at which the loss peaks occur [42]. Zheng and Wong report on blends of PMMA with graphite and with expanded graphite. The conductivity of these blends is determined using a four-point probe measurement and the dielectric measurements are taken using a dielectric analyzer. The conductivity of the blend with graphite is 10^{-5} S/cm and with expanded graphite is 10^{-4} S/cm and the loss factor is a function of both frequency and temperature [47]. Zidan and Abu-Elnader discuss the optical effects of doping on PMMA films. The intensity of the absorption bands is seen to increase with increasing dopant levels, and the reflection increases and transmission decreases as the wavelength increases [48].

2.1.5 Polycarbonate

Polycarbonate is a linear, polycrystalline material. The dielectric behavior is reported by El-Shabasy and Riad over the temperature range of 297 K to 365 K and the frequency range of 30 Hz to 100 kHz, and relative dielectric constant versus dielectric loss as a function of frequency is plotted for different temperatures. The I-V characteristics of polycarbonate show no rectifying behavior [49]. Reed *et al.* report on using polycarbonate as a temporary layer that is destroyed later on in the fabrication process in order to fabricate microchannels [11].

Amorphous polycarbonate (APC) is a polar polymer that can be doped and is typically prepared in cyclopentanone. Hayden *et al.* report that APC has good electrical and mechanical properties up to high temperatures, high continuous service temperatures, reasonable optical clarity, low moisture absorption, and resistance to water, acids, oxidizing and reducing chemicals. High-quality thin films of APC are formed by spin-coating onto the desired wafer. Hayden *et al.* also find that APC dopes well with a variety of nonlinear optical chromophores [50]. Santos *et al.* report the complex dielectric measurement curves from 12 Hz to 10 kHz at room temperature for 10 micron thick APC thin films, and the related conductivity curves are also obtained [51]. APC has been used in the fabrication of low-voltage EO modulators, with high temperature stability and low optical loss, at room temperature [52].

2.2 New polymer dielectric materials

There are polymer and biopolymer materials that have yet to be studied in depth. This section reviews the literature on new biopolymers based on deoxyribonucleic acid (DNA) and bovine serum albumin (BSA).

2.2.1 DNA-biopolymer

The salmon-based DNA-biopolymer is made from purified waste products of the Japanese fishing industry, specifically the salmon roe and milt sacs. This water-soluble DNA is sonicated to the desired molecular weight, if necessary, and then is precipitated with a cationic surfactant, such as hexadecyltrimethylammonium chloride (CTMA), to create a biopolymer. This biopolymer is water insoluble and more mechanically and thermally stable than a pure DNA thin film [53, 54].

The resistivity of DNA-CTMA thin films hardened with the crosslinker poly(phenyl isocyanate)-co-formaldehyde (PPIF) are carefully measured as a function of temperature using a guarded electrode configuration along with an alternating polarity measurement technique. The resistivity of crosslinked DNA-CTMA films is seen to decrease from $10^{14} \Omega\text{-cm}$ at 23°C to $10^9 \Omega\text{-cm}$ at 100°C , and the resistivity is not affected by the addition of a small amount of the chromophore disperse red 1 (DR1) [55]. The DNA-biopolymer also has a unique double-helical structure which could be beneficial to electro-optic applications using this biopolymer film [12].

Although the DNA-biopolymer is a relatively new material, several thin-film devices are reported in the literature. One of these is a DNA-biopolymer based organic light emitting diode (BioLED). For these devices low molecular weight (about 145 kDa) DNA-biopolymers serve as an electron blocking layer. The luminance of these BioLEDs is increased by a factor of two [14]. Another DNA-biopolymer thin-film device is the DNA-based waveguide. Heckman *et al.* report that the DNA-biopolymer is suitable for a core layer in a waveguide because of its low optical absorption loss. Crosslinking DNA-CTMA yields a material that is stronger and more resistant to the solvents used in processing DNA-CTMA films than DNA-CTMA that has not been crosslinked [53]. The index of refraction of DNA-CTMA can be altered by the addition of DR1 to produce the higher index of refraction needed for use as a core layer in an all-DNA waveguide [12]. A third device is the DNA-biopolymer gate dielectric in an organic field effect transistor, called a BioFET [15, 16]. Using a high molecular weight DNA-biopolymer as the gate dielectric, steady state current-voltage measurements and the dielectric response are determined at low frequencies. A sizeable hysteresis exists for drain current as a function of gate voltage. With a gate voltage of less than ten volts, the BioFET modulates the drain current by more than three orders of magnitude [15, 16]. Together, these devices show that DNA-biopolymer electronics are possible.

2.2.2 BSA-biopolymer

The biopolymer bovine serum albumin polyvinyl alcohol is known as BSA-PVA. BSA is a common globular protein extracted from cow's blood. In order to enhance the mechanical and thermal properties of the material a plastisizer is added [41]. This is similar to what is done when the surfactant CTMA is added to DNA. The plastizer used for this work is polyvinyl alcohol (PVA) [41]. BSA-PVA is a unique combination of materials generated by Dr. Lawrence Brott in the Biotechnology Group in the Materials and Manufacturing Directorate of the Air Force Research Laboratory (AFRL) located at Wright Patterson Air Force Base in Ohio.

2.3 Microwave characterization

Microwave characterization is the process by which properties of the material of interest are determined at microwave frequencies (typically defined as 300 MHz to 300 GHz). It is also a study of how the material of interest reacts to microwave inputs. For the purpose of this dissertation, the materials of interest are polymer and biopolymer thin films. The microwave characterization in this study is an indirect, broad-band measurement of the dielectric properties, specifically the relative dielectric constant and loss tangent, of these thin films.

One general method of determining the relative dielectric constant and loss tangent over a broad band frequency range involves obtaining the S parameter measurements and then using appropriate data processing to obtain the dielectric parameters from the measurements. This general method is reported in the literature for various test structures and data processing techniques. One such technique involves the measurement of a microstrip test device where a portion of the microstrip line is covered with the isotropic sample [56] or composite polymer [57] being tested. Determining the dielectric properties from the measured S parameters using this technique involves an electromagnetic

analysis of the microstrip line along with an optimization program [56]. A second technique consists of measuring a TEM transmission line or waveguide in which a portion of the device contains the sample under test. From the measured S parameters, the reflection coefficient and propagation factor at the interface between the material-filled and air-filled device are computed and then the dielectric properties of the device are computed [58].

A second general method incorporates thin films into microstrip transmission lines to determine their permittivity. The technique consists of measuring both a reference set and the desired set of microstrip transmission lines for both the propagation constant and the characteristic impedance. This separates the electrical properties of the dielectric thin film from those of the conductor, and yields a more accurate value for the relative dielectric constant of the thin film [59].

A third general method also compares the propagation characteristics of a reference sample with those of the desired sample. This method determines both the relative dielectric constant and the loss tangent of the thin film. This technique uses a coplanar waveguide transmission (CPW) line with ground, signal, and ground electrodes. From the S parameter measurements of the CPW line, the capacitance of each sample is determined. From the capacitance and impedance values, the relative dielectric constant and loss tangents are calculated [60].

A fourth general method uses interdigitated capacitors fabricated on the thin film. The capacitance and loss tangent of the film are measured using an impedance analyzer, and the dielectric quality factor is obtained from the single port S parameter measurements [61, 62]. The relative dielectric constant is calculated by a conformal mapping technique from the measured capacitance value accounting for the relative dielectric constant of the substrate material [63].

2.4 Field effect transistors

Field effect transistors (FETs) are three terminal devices that use a small input signal to control a large output [64]. The three terminals of the FET are typically called the gate, source and drain. The source and drain are connected by an active channel through which charges flow when the transistor is active. The maximum amount of charge that flows through the channel at any particular time is controlled by the voltage applied to the gate. FETs can operate in two device modes, called enhancement mode and depletion mode. A depletion mode, or normally on, FET has a large channel where current is free to flow when there is no gate bias applied. Therefore in order to stop the flow of current through a depletion mode FET, a negative or positive bias is used to deplete the channel of carriers [65]. The pinch-off voltage in a depletion mode FET is the voltage that causes the channel to be completely shut-off, and current no longer flows. In a depletion mode FET, applying a negative or positive bias to the gate causes the channel to constrict such that less current flows. An enhancement mode, or normally off, FET has no current flowing when there is no gate bias; therefore for current to flow, a channel first needs to be induced [65]. The threshold voltage in an enhancement mode FET is the voltage where the transistor changes from having no current flowing in the channel to having current flow. In an enhancement mode FET, applying a bias with a greater magnitude than the threshold voltage to the gate causes the channel to expand such that more current flows.

The FETs of interest in this dissertation are those that have one or more polymer layers. Polymers can be used for any part of a FET. When a polymer is part of a FET, the FET is often referred to as a polymer FET, an organic FET, or a thin film transistor (TFT). When the term TFT is used for a FET containing a thin film polymer layer, most often the thin-film is in the semiconducting layer.

2.4.1 Polymer FETs

Polymer FETs include polymers in any region of a FET, from the semiconducting layer to the electrodes. Yamamoto *et al.* examine a spin-coated polymer semiconducting layer made of copolymers in which standard transistor behavior is observed. Copolymers are polymers that are capable of operating in both n-type and p-type FETs [66]. TFTs using semiconducting polymers show that performance is dependent upon polymer film thickness [67]. Polymers can be used as gate dielectrics, but this has caused a large hysteresis in the transfer characteristics. Uemura *et al.* report that using a layer of mineral clay to protect the semiconductor layer eliminates the hysteresis [68]. The mobility of FETs with polymer insulators is affected by the specific polymer used [69]. Ashizawa *et al.* report on successfully fabricating and testing FETs where the source, drain, and gate electrodes and also the channel are made of the same doped conducting polymer. The FET is normally on, with a positive gate voltage causing it to act in the depletion mode [70]. Thin film polymer FETs have also been used for optical emission applications. The gate bias controls the location of the light emission [71, 72]. In these light emitting FETs, high performance is obtained from the simultaneous injection of holes from the drain and electrons from the source [72].

2.4.2 All-polymer FETs

All-polymer FETs are typically fabricated by spin-coating, vapor deposition and other common lithography techniques with all layers made from polymer materials. They are shown to be stable in air without protective coatings which is important for low-cost, high volume applications [73]. In comparing all-polymer FETs to fully inorganic FETs by changing one layer at a time of the inorganic FET to a polymer material, it is reported that very slight degradation of performance is seen when the polymer layer replaces the silicon substrate and oxide layer [74]. Organic FETs need to be

lightweight, thin and pliable to obtain flexible electronic devices. Pliable materials need to be used for the active and insulating layers in order to achieve this [75]. Thin film semiconducting polymers can be used as the active material in FETs. However, undoped semiconducting materials have high resistivities. Edman *et al.* report that doped semiconducting polymers have lower resistivities, and higher doping levels yield lower resistances. Therefore, polymers with high electron and hole mobilities that can support doping are useful for transistors [76].

2.4.3 Sensor applications

Many polymer FETs described in the literature are used for sensing applications. Sensors are devices that measure a particular signal, such as voltage, temperature, gas, and light. Krishna *et al.* describe a polymer FET with a conducting polymer gate that is fabricated as a chemical sensor using standard complimentary metal-oxide-semiconductor (CMOS) processing [77]. Kazanskaya *et al.* report on FET based sensors with a polymer membrane that works as a potentiometric sensor detecting ammonium ions or as a biosensor detecting urea. The polymer membrane used with this sensor is light sensitive and its elements are easily changed so that it can detect a variety of biological substances [78]. Dutta and Narayan report on a polymer FET that detects light and operates as a memory device. Information is optically introduced and electrically removed from this FET [79]. Deen and Kazemeini describe the use of photosensitive semiconducting polymers in photodetectors. These photodetectors are highly sensitive with no gate bias [80]. The low cost and comparable semiconducting characteristics of polymer semiconducting materials to silicon make their use appealing for sensor applications. However, polymer semiconducting materials tend to have low mobility and strong temperature dependence [81], which may not be ideal for some sensor applications.

Conducting polymers are typically the active gate material in gas or vapor sensors. They operate at room temperature, consume lower power than non-polymer based FET sensors and are dependent upon the humidity present [82]. They are more sensitive than resistive gas sensors and they respond quickly [83]. Using composite conducting polymers prevents humidity from affecting the magnitude of the response but shows significant unwanted temperature dependence. It is easy to combine the polymer deposition with current CMOS technology [84].

2.5 Summary

This chapter covers a substantial range of background information from existing and well studied polymer dielectric materials to existing information on new biopolymers, to existing microwave characterization techniques, to applications for polymer based dielectric materials. Relatively little research has been done on the electrical properties of biopolymers and on applications using these biopolymers, as these biopolymers are just starting to be characterized and studied.

The next chapter describes the processing techniques used in this dissertation. Included in these techniques are the methods used to create the DNA-biopolymers, the biological technique commonly used to determine the molecular weight of the DNA, and thin film deposition techniques. Some of these techniques are well-known, but problems are encountered when using the standard techniques with the new biopolymer materials. Some of these problems and useful solutions to them are also described in the next chapter.

CHAPTER III

BIOPOLYMER PROCESSING TECHNIQUES

This chapter describes the processing techniques that are used to create the DNA-based devices used in this dissertation. First, the processing of the DNA-based material from the raw materials is explained. Next, the technique used to determine the average molecular weight of DNA is described. Finally, the deposition techniques of spin-coating and molecular beam deposition are explained.

3.1 DNA-based biopolymers

The DNA used in these devices is processed from purified DNA provided by the Chitose Institute of Science and Technology (CIST) [54, 85]. This DNA comes from the waste products of the Japanese fishing industry, specifically that of the salmon roe and milt sacs. The DNA is extracted from the waste products by an enzyme isolation process, and is purified by CIST. The purified DNA obtained from CIST has an average molecular weight that is between six and eight million Daltons (6000 - 8000 kDa). Several unique processing techniques have been developed to make biopolymers that are useful for device fabrication from the purified DNA.

3.1.1 DNA-CTMA

Heckman *et al.* describe a technique to obtain low molecular weight DNA-CTMA. First, two grams of DNA are dissolved in 500 mL of deionized water to produce a concentration of four grams

per liter. This beaker of dissolved DNA is then placed into a bucket and the beaker is surrounded by ice to prevent overheating. Then a Sonics & Materials ultrasonic processor model VC-750 with a 19 mm diameter high gate solid probe is used in pulse mode to reduce the molecular weight of the DNA from 6000 - 8000 kDa to the desired molecular weight. Each pulse consists of sonicating for ten seconds and resting for twenty seconds. For this research, the desired average molecular weights are 1000 kDa and 300 kDa, which require sonicating the dissolved DNA for two and ten nine-minute cycles, respectively. Each nine-minute sonication cycle releases around 20 kJ of energy into the dissolved DNA. The sonicated DNA is filtered through a 0.65 micron nylon filter, and then is titrated into CTMA that is dissolved in deionized water. After mixing for four hours, the precipitate settles out of the water. This precipitate is then thoroughly rinsed and dried overnight in a vacuum oven. This renders a water-insoluble complex of DNA-CTMA that can be dissolved in many of the alcohols, including butanol and methanol, and that can be spin-coated into a thin-film [53].

3.1.2 DNA:PEDOT:CTMA

A processing technique similar to that used to create DNA-CTMA is outlined by Hagen *et al.* to obtain DNA:PEDOT:CTMA [86]. This biopolymer is formed from the raw DNA obtained from CIST, poly(3,4-ethylenedioxythiophene) poly(styrenesulfonate) (PEDOT:PSS), and CTMA. The aqueous dispersion of PEDOT:PSS is commercially known as Baytron P. In this work, two grams of DNA are dissolved in 500 mL of deionized water to produce a concentration of four grams per liter for sonication. This beaker of dissolved DNA is then placed into a bucket and the beaker is surrounded by ice to prevent overheating. Then a Sonics & Materials ultrasonic processor model VC-750 with a 19 mm diameter high gate solid probe is used in pulse mode for ten nine-minute cycles to reduce the molecular weight of the DNA from 6000 - 8000 kDa to an average molecular

weight of about 300 kDa. Each pulse consists of sonicating for ten seconds and resting for twenty seconds. Each nine-minute sonication cycle releases around 20 kJ of energy into the dissolved DNA. After sonication is complete, the dissolved DNA is filtered through a 0.65 micron nylon filter. Baytron P is purified before titration by filtering through a 0.45 micron polytetrafluoroethylene (PTFE) syringe filter. Then, 17.0 grams are added dropwise to the dissolved DNA at a ratio of approximately 1:80 PEDOT molecules to DNA base pairs. This is equivalent to adding 36.0 wt% of PEDOT molecules into the DNA, or 89.9 wt% Baytron P into the DNA. The DNA:PEDOT solution is mixed with a magnetic stirrer at room temperature for four hours. An excess amount of CTMA is dissolved in deionized water. The CTMA solution is then slowly poured into the DNA:PEDOT solution, as it is being stirred, keeping the stream of CTMA solution as small as possible. This results in the DNA:PEDOT:CTMA complex. The DNA:PEDOT:CTMA solution stirs for two hours, and afterwards the precipitate settles out of the water. Finally, the precipitate is thoroughly rinsed and dried overnight in a vacuum oven. This renders an organically soluble, semiconducting complex of DNA:PEDOT:CTMA.

3.2 Agarose Gel Electrophoresis

Agarose gel electrophoresis is a biological technique commonly used to separate and identify DNA fragments by the number of base pairs (bp) present [87]. The molecular weight is equal to the number of base pairs in the strand of DNA times 660 g/mol/bp. Applying an electric field to an agarose gel that has at least one sample containing DNA loaded in it causes the negatively charged DNA fragments to move towards the positive lead. When the electric field is removed, the smaller fragments have moved farther through the gel than the larger ones. A 1000 base pair DNA ladder, shown in Figure 3.1, is a sample of DNA that contains many known DNA base pairs up to 1000

base pairs. By loading a DNA ladder into the agarose gel along with the DNA samples of interest, the number of base pairs present in the samples can be determined by comparing the distance each sample traveled to the loaded DNA ladder.

Agarose is a powder that is made from seaweed. This powder is mixed with a 10x TAE (Tris-acetate and ethylenediamine tetraacetic acid) buffer solution to make a 0.8% agarose gel. In order to dissolve the agarose, the solution is heated to boiling and mixed. After the agarose has dissolved, the solution is cooled for several minutes. Once the container that contains the agarose gel is just warm to the touch, a very small amount of ethidium bromide, a fluorescent dye, is mixed in. Then, the gel is poured into the gel holder taking care not to overfill it. After the gel has solidified, the well holder is removed. A 1x TAE buffer is poured over the gel to completely cover it. Five microliters of ethidium bromide are then added to the buffer and the gel holder is moved around until the ethidium bromide disappears. The 1 Kbp DNA ladder is mixed with the DNA loading dye at a ratio of 1:2, and is entered into the first well. Each sample, which consists of an aqueous solution of DNA in deionized water at a concentration of 1 g/2 L, is mixed with the DNA loading dye at a ratio of 1:2 and is entered into other wells. After all the wells have been loaded, the gel is connected to a voltage source with the positive lead farthest from the wells to encourage the DNA to migrate across the gel. A constant voltage of 100 V is applied until the dye has propagated across the gel, but not off the far end. The gel is then removed from the gel holder, placed under a UV lamp, and a picture is taken of the DNA strands. The brightest spot for each sample is the largest concentration of DNA, and that spot is compared to the DNA ladder to determine the number of base pairs of the sample.

A Matlab graphical user interface (GUI) has been written to easily obtain the brightest spot in each sample and to calculate the mode of the molecular weight distribution from the image file of the picture taken from agarose gel electrophoresis. The user identifies various points that have the same

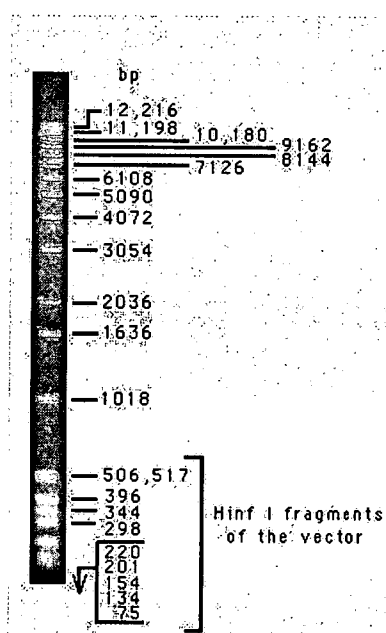


Figure 3.1: The 1 Kbp.DNA ladder, as seen in standard literature.

number of DNA base pairs on both the reference ladder in the agarose gel and the standard DNA ladder, in order to align the two ladders. This alignment is required to determine the number of DNA base pairs and hence the molecular weight of the DNA present at any location in the agarose gel output. Once this alignment is complete, the molecular weight of the DNA present at the brightest spot in each sample can be determined. The final output of this script is shown in Figure 3.2. The mechanical chopping of DNA by the ultrasonic processor produces a large distribution of molecular weights within a single sample of DNA, which yields the large distribution of base pairs seen in the image, as shown in Figure 3.2. The X's show the location in the distribution for the listed molecular weight value. A figure that shows the alignment between the ideal DNA ladder and that of the loaded DNA ladder that has been matched to it, is also produced as output.

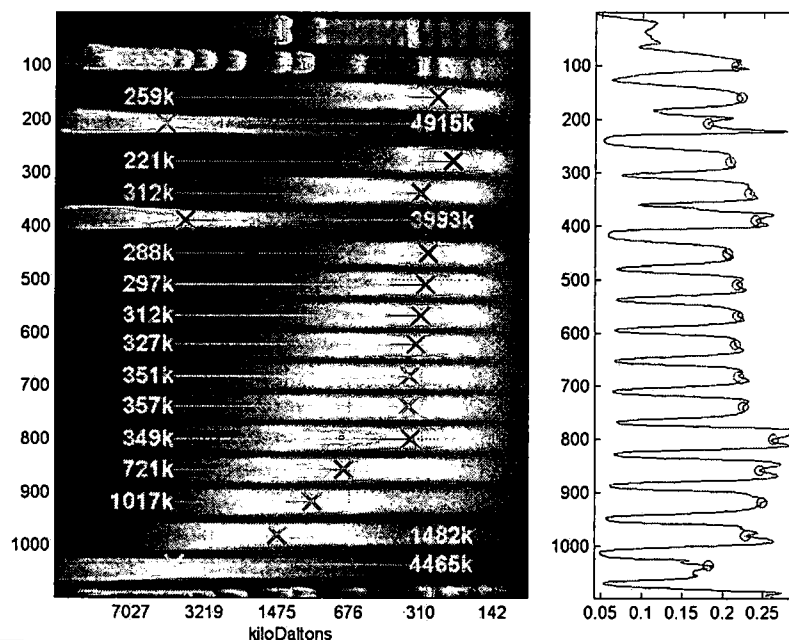


Figure 3.2: Results of an agarose gel electrophoresis run with the determined molecular weight values superimposed on top.

3.3 Thin-film deposition

There are numerous ways to obtain a thin-film of polymer, including spin-coating, flow-coating, and molecular beam deposition. The deposition techniques used in this research are spin-coating and molecular beam deposition. Spin-coating is used to make films that are at least 100 nm thick, while molecular beam deposition is used for very thin films no greater than 100 nm. This section describes both of these methods, and the specific parameters used in each.

3.3.1 Spin coating

Spin coating is a standard method used to apply uniform, polymer based films of a desired thickness across an entire wafer or substrate. The polymer is first dissolved in a solvent, such as butanol

or cyclopentanone, and mixed by an ATR Rotamix tumbling mechanism until fully dissolved. For most polymers, the polymer is fully dissolved after an hour or two of mixing and when no polymer pieces remain visible in the solution, but the DNA-biopolymers need to be mixed for at least six hours to equally distribute the various DNA chain lengths and obtain uniform films by spin-coating. Then, the polymer solution is filtered through a 0.2 micron PTFE syringe filter. Finally, the solution can be deposited by spin coating onto the desired substrate.

Wolf and Tauber describe the three stages of the spin coating procedure for photoresist, which are the same stages used to spin coat polymers [88]. First, the solution is dispensed onto the substrate. Then the wafer is accelerated to the desired spin speed in a designated amount of time. Finally, the wafer spins at the desired speed for a specific amount of time to obtain the desired thickness and evaporate the solvent. For standard polymers, film uniformity is improved by keeping the acceleration time to a minimum. For DNA-CTMA, however, this is not the case. As Heckman describes, using a five second ramp when spin coating DNA-CTMA films increases the film uniformity [89]. Using a ten second ramp is beneficial when spin coating films at speeds greater than 2000 RPM due to the multiple steps needed to obtain speeds greater than 2000 RPM.

Adhesion is a problem for polymer films obtained by spin coating at room temperature. Poor adhesion of the film to the substrate will cause problems, such as pinholes and non-uniform thicknesses, for devices built from these films. Therefore, when spin coating DNA-CTMA or APC onto a substrate, care must be taken to promote the adhesion of the film onto the substrate. It has been found that heating the substrate before dispensing the polymer promotes better adhesion, as does heating the polymer solution.

APC film thickness is shown in Table 3.1 as a function of the concentration in cyclopentanone and the spin parameters used. This table shows that higher concentrations and slower spin speeds

produce thicker films. Using the same spin and ramp speeds with DNA-CTMA will not produce the same film thicknesses as both the viscosity of the solutions and solvents used are different. DNA-CTMA is nonsoluble in cyclopentanone, but is soluble in various alcohols. Butanol is the solvent of choice for spin coating DNA-CTMA due to its high boiling point, which causes it to evaporate more slowly producing more uniform thin-films. DNA-CTMA film thickness for average molecular weights of 300 kDa and 1 million Da are shown in Tables 3.2 and 3.3 as a function of concentration in butanol and the spin parameters used.

After spinning the polymer film, the substrate is removed from the spinner and placed in an oven set to a constant temperature of 70 °C for about two hours to promote the evaporation of any remaining solvent and allow the film to harden. For the DNA-biopolymers, this oven should have a nitrogen flow on it to prevent moisture from being absorbed by the film while it is drying.

3.3.2 Molecular Beam Deposition

Molecular beam deposition (MBD) is another method of depositing DNA-biopolymer thin films. This method is a thermal evaporation technique that takes place in high vacuum. The vacuum allows for a molecular beam with minimal scattering. The deposition rate varies based on the material being deposited, and the amount of material in the crucible, but not on the temperature of the system. The crucible containing the material to be deposited is placed into a small furnace adjacent to the high vacuum chamber where the substrate being deposited on is held [90]. A shutter separates the furnace from the vacuum chamber to prevent deposition from starting before the desired deposition temperature is reached. Once the desired temperature and vacuum pressure are reached, the shutter is opened and deposition onto the sample begins. The films deposited by MBD in this research are 50 nm thick, the deposition temperature is 140 °C, and the base pressure is 10^{-6} Torr.

Table 3.1: Parameters used to obtain APC films from APC dissolved in cyclopentanone

Weight percent	Spin speed	Spin time	Approximate film thickness
5 wt%	1000 RPM	10 s	0.5 μm
10 wt%	2700 RPM	10 s	1.0 μm
10 wt%	1250 RPM	10 s	1.5 μm
12 wt%	3000 RPM	10 s	1.5 μm
12 wt%	1500 RPM	10 s	2.0 μm
12 wt%	1250 RPM	10 s	2.5 μm
12 wt%	1000 RPM	10 s	3.0 μm

Table 3.2: DNA-CTMA thin films from DNA-CTMA dissolved in butanol made from 300 kDa DNA

Weight percent	Ramp time	Spin speed	Spin time	Approximate film thickness
5 wt%	5 s	500 RPM	40 s	0.5 μm
10 wt%	5 s	1500 RPM	40 s	1.0 μm
12 wt%	5 s	1500 RPM	40 s	1.5 μm
12 wt%	5 s	1000 RPM	40 s	2.0 μm
12 wt%	5 s	500 RPM	40 s	2.5 μm

Table 3.3: DNA-CTMA thin films from DNA-CTMA dissolved in butanol made from 1000 kDa DNA

Weight percent	Ramp time	Spin speed	Spin time	Approximate film thickness
5 wt%	10 s	5000 RPM	40 s	0.25 μm
5 wt%	5 s	1000 RPM	40 s	0.5 μm
10 wt%	5 s	3000 RPM	40 s	1.0 μm
10 wt%	5 s	1500 RPM	40 s	1.5 μm
10 wt%	5 s	500 RPM	40 s	2.5 μm

3.4 Summary

This chapter presents the processing techniques used to create the thin films used in this dissertation. The procedures used to take the purified DNA and make DNA-CTMA and DNA:PE-DOT:CTMA are described, along with the techniques and software used to determine the molecular weight of the DNA to be included in these biopolymers. Some of the unique problems encountered and various solutions that were used in depositing uniform thin films, along with the method used to determine the average molecular weight of DNA are described.

The next chapter describes a new capacitive test structure that is designed to characterize biopolymer films at microwave frequencies. The structure, fabrication process, and electrical model will be presented. Microwave and low frequency measurements will be described and the results discussed. Also, electric field microscopy and the obtained images will be described.

CHAPTER IV

ELECTRICAL CHARACTERIZATION OF BIOPOLYMERS

This chapter describes the electrical characterization of several polymers. The first part of this chapter describes new microwave frequency polymer characterization work, and the second part describes some low frequency electrical measurements using the same test structure and polymers. The first part begins with a description of the new capacitive test structures used for this characterization. Then, the design of and fabrication procedure for these capacitive test structures are described. Third, the electrical model is shown and the S parameters are algebraically defined. Fourth, the experimental procedure is outlined and the analysis is described. Finally, the microwave results obtained are presented and analyzed for the various polymers and compared to a known ferroelectric material. The second part of this chapter begins with a description of the capacitive measurements taken at low frequencies and a description of the resulting measurements. Then, electric force microscopy (EFM) measurements are described and the results obtained are presented and analyzed.

4.1 Capacitive Test Structure

A new capacitive test structure is used to characterize the electrical properties of polymer and biopolymer thin films. Specifically, this capacitive test structure provides a mechanism for determining the dielectric properties of polymer and biopolymer materials in an easily fabricated device.

The dielectric properties obtained using the capacitive test structure are determined from microwave measurements.

The capacitive test structures used in these studies are fabricated on a two-inch wafer of high resistivity silicon using shadow masks and spin-coating. The capacitive test structure is shown in Figure 4.1. This structure is made up of four distinct layers on the silicon wafer. The adhesion layer consists of 100 Å of chromium sputtered through a shadow mask directly onto the silicon wafer. The bottom metal layer, which is formed from 7500 Å of gold deposited by electron beam (e-beam) deposition through the same shadow mask onto the adhesion layer, consists of two ground lines shunted together at their midpoints by a 100 μm wide conductor in the shape of an H. The next layer is the polymer under study, which is deposited as a thin-film by spin-coating on top of the gold. The top layer is 3500 Å of gold, deposited by e-beam deposition through a second shadow mask. This layer forms a ground-signal-ground coplanar waveguide (CPW) transmission line. The CPW line consists of two ground lines, positioned directly above the ground lines in the bottom metal layer, and a signal line, centered between the ground lines and perpendicular to the shunt line in the bottom metal layer. The active region of this test structure is the area where the signal line in the top metal layer overlaps the shunt line in the bottom metal layer. The active region forms a test capacitor, which has an area of approximately 100 μm by 100 μm . The test structure has a large ground pad capacitor that results from the overlap of the ground lines in the top and bottom metal. Since the test capacitor is in series with the much larger ground pad capacitor, the effective capacitance is that of the test capacitor. When a DC bias is applied, the DC current passes through the leakage conductance of the test capacitor, the shunt line in the bottom metal and the leakage conductance of the ground pad capacitor. This eliminates the need for via holes to ground the bottom conductor. Since the large ground pad capacitor has a much higher leakage conductance,

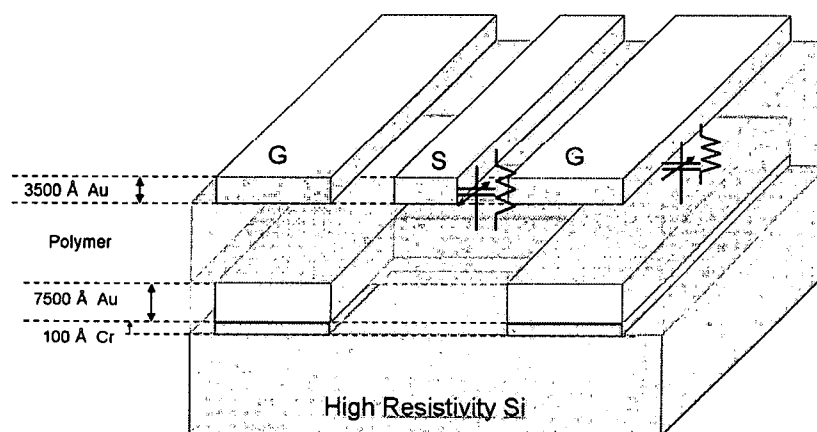


Figure 4.1: A three dimensional representation of the capacitive test structure, showing the overlap of the signal conductor in the top-metal and the shunt line in the bottom metal which form the test capacitor. Notice that the large ground pad capacitor is in series with the test capacitor, resulting in the equivalent capacitance of the test capacitor.

the DC bias applied to the signal conductor drops almost entirely across the test capacitor. Figure 4.2 shows a photograph of the capacitive test structure being measured.

An electrical model of the capacitive test structure is shown in Figure 4.3. In this model, $C(V)$ is the test capacitance of the polymer in the active region, and $R(V)$ is the shunt resistance modeling the leakage conductance of the test capacitor. R_S and L are the parasitic series resistance and inductance, respectively, for the test capacitor. Using this electrical model and the scattering parameters (S parameters), the relative dielectric constant (ϵ_r) and loss tangent ($\tan \delta$) of the polymer can be derived as described below.

Since this system is a two-port reciprocal network, deriving the S parameters amounts to deriving S_{11} and S_{21} . For any reciprocal two-port network S_{11} is identical to S_{22} and S_{21} is identical to

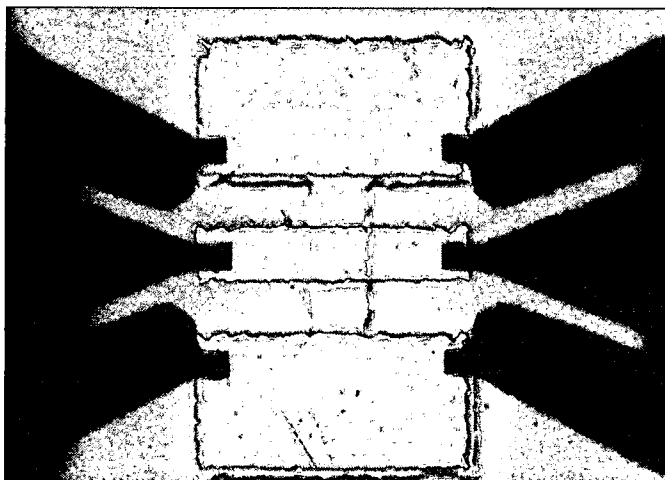


Figure 4.2: A photograph of a capacitive test structure with the CPW probes in place to make microwave measurements.

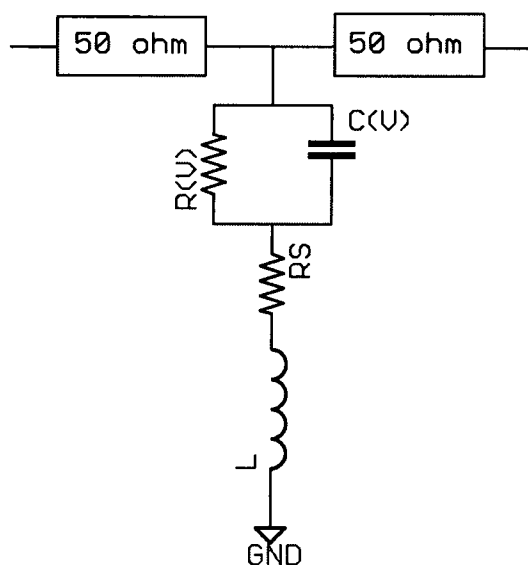


Figure 4.3: The electrical model for the capacitive test structure.

S_{12} . Any single S parameter, S_{ij} , is defined as

$$S_{ij} = \frac{V_i^-}{V_j^+} \quad (4.1)$$

where V_j^+ is the amplitude of the wave incident on port j and V_i^- is the amplitude of the wave reflected out of port i [91]. This is determined when the only incident wave in the system is that incident upon the input port, port j , and all other ports are terminated with matched loads to avoid reflections. For the two-port network that describes the capacitive test structure, with port 1 as the input port and port 2 as the output port, it can be shown that

$$S_{11} = \frac{Z_{in}^1 - Z_0}{Z_{in}^1 + Z_0} \quad (4.2)$$

and

$$S_{21} = \frac{v_o}{v_{in}} \quad (4.3)$$

where Z_{in}^1 is the impedance seen looking into port 1 and Z_0 is the characteristic impedance of the transmission line. To algebraically calculate the S parameters for the capacitive test structure, one must account for the loss associated with the real transmission line. In this case, the loss associated with each 50 Ω transmission line is assumed to be 1 Ω . Using Figure 4.3 and the characteristic impedance $Z_0 = 50 \Omega$, Z_{in} and the S parameters for the capacitive test structure can be computed as

$$S_{11} = \frac{2R + 2jwL + 2(\frac{1}{R} + jwC)^{-1} - 2499}{102R + 102jwL + 102(\frac{1}{R} + jwC)^{-1} + 2601} \quad (4.4)$$

and

$$S_{21} = \frac{50[R + jwL + (\frac{1}{R} + jwC)^{-1}]}{51[51 + R + jwL + (\frac{1}{R} + jwC)^{-1}]} \quad (4.5)$$

The relative dielectric constant, ϵ_r , is determined from the capacitance in the electrical model.

The capacitance is that of the parallel plate capacitor consisting of the polymer film in the active

region. Manipulating the equation for the capacitance of a parallel plate capacitor, the relative dielectric constant can be computed as

$$\epsilon_r = \frac{C(V)t}{\epsilon_o A}, \quad (4.6)$$

where $C(V)$ is the capacitance, ϵ_o is the permittivity of free space, A is the overlap area of the active region, and t is the thickness of the polymer. The loss tangent [91] is found from the electrical model of the capacitive test structure, using the equation for the shunt resistance such that [92]

$$\tan(\delta) = \frac{1}{\omega R(V)C(V)}, \quad (4.7)$$

where ω is the angular frequency, $R(V)$ is the shunt resistance, and $C(V)$ is the capacitance shown in Figure 4.3 at a single bias voltage.

4.2 Experimental Procedure

The specific values for the parameters in the electrical model are determined experimentally by fitting the circuit model to the experimentally obtained S parameters using the simulation package in Applied Wave Research's (AWR) Microwave Office® tools. A Hewlett Packard 8720B Microwave Network Analyzer and an on-wafer microwave probe station, shown in Figure 4.4, are used to measure the S parameters of the capacitive test structure. The setup used to measure the S parameters is the same two-port network, with one port at each end of the signal line, as is described above for the theoretical calculations. The procedure for experimentally determining the S parameters in this study uses the following steps: First, the network analyzer and probe station are calibrated to the device over the frequency range of interest using a Line-Reflect-Reflect-Match (LRRM) calibration [93]. The frequency range of interest for this work is five to twenty gigahertz, when the data is taken at the Sensors Directorate of the Air Force Research Laboratory, since conductive thickness effects

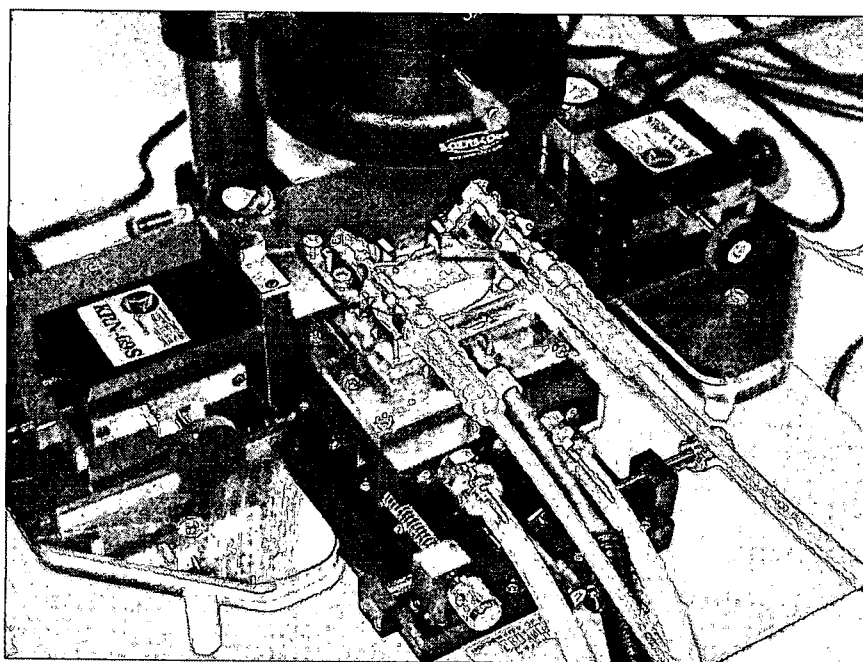


Figure 4.4: The microwave probe station pictured with the right probe on a capacitive test structure containing BSA-PVA and the left probe hovering above the sample.

cause skin depth issues that limit the low frequency and equipment limitations restricts the high frequency, and ten to eighteen gigahertz, when the data is taken at the University of Dayton, also due to equipment limitations. Then, the silicon wafer is raised to the temperature of interest and the appropriate DC bias voltage is applied to the signal lead of the probe. Finally, the S parameters are recorded.

The measured S parameters are then imported into the AWR Microwave Office® simulation package. Using the electrical model for the test structure, shown in Figure 4.3, the electrical parameters are determined. First, an initial estimate of the values in the electrical model of the capacitive test structure is made. Then, the electrical model is manually tuned to match the experimental results for both S11 and S21, simultaneously, across the frequency range. This procedure is repeated

for each capacitive test structure at every bias voltage and temperature yielding the specific values for the electrical model. Since there are four parameters ($C(V)$, $R(V)$, R_S , and L) in the electrical model that are being varied to match the experimental data, using just the S21 or S12 curve can result in several matches that appear to be good. However, using both the S21 (or S12) curve and the S11 (or S22) curve generally produces a unique electrical model that matches both curves well. Figure 4.5 shows an example of the AWR Microwave Office screen while matching the electrical model to the experimental data. The electrical model is seen on the top right, with the variable tuner

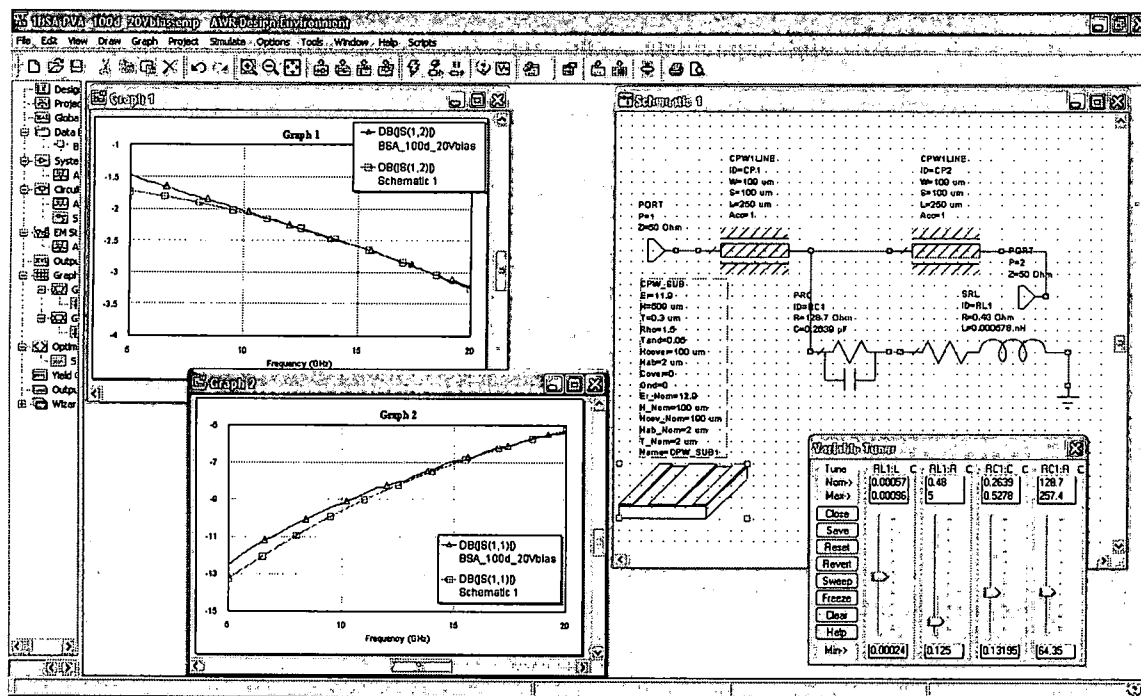


Figure 4.5: An example of the AWR Microwave Office screen while matching circuit parameters with the measured S parameters. The graphs of S11 and S12 with both experimental and theoretical data from the model are seen on the left side of this figure. The electrical model and the variable tuner are seen on the right side of this figure.

below it. The S12 graph containing both the experimental data and the theoretical data is seen on the top left and the S11 graph is visible on the bottom left.

4.3 Results and analysis

The polymer poly(bisphenol A carbonate-co-4,4'-(3,3,5-trimethylcyclohexylidene)diphenol carbonate), commonly known as APC, is used as a reference polymer for comparison to two biopolymers, DNA-CTMA and BSA-PVA. Additionally, a film of polyvinyl alcohol (PVA) is used to determine if the results of BSA-PVA are due to the PVA or the biologically-based BSA. A summary of the microwave dielectric properties for these polymers is contained in Table 4.1.

Variations in the S21 measurements are found to occur for different capacitive test structures on the same substrate. This is presumably due to thickness variations in the thin films, which cause different thicknesses in the active region of the various capacitive test structures containing the thin film. Since it is not possible to measure the thickness of the film for a particular test structure, the average film thickness is used to obtain the dielectric properties. The average thickness of the APC film is $2.03\ \mu\text{m}$, of the BSA-PVA film is $2.33\ \mu\text{m}$, and of the DNA-CTMA film is $1.78\ \mu\text{m}$. From the collection of measurements obtained, the mean relative dielectric constant and mean loss tangent at 15 GHz are computed and reported in Table 4.1.

Table 4.1 shows that the mean relative dielectric constant for the materials measured ranges from 4.7473 for APC at $100\ ^\circ\text{C}$ to 6.9456 for BSA-PVA with no applied bias at $100\ ^\circ\text{C}$. The mean loss tangent at 15 GHz ranges from 0.1288 for PVA, with no applied bias at room temperature, to 0.3477 for BSA-PVA, with 20.0 V applied at room temperature. BSA-PVA has the highest mean relative dielectric constant for every condition, while APC has the lowest mean relative dielectric constant. This shows that biopolymers have higher relative dielectric constants than the reference polymers

Table 4.1: The mean microwave dielectric properties calculated from the S parameter measurements for APC, PVA, BSA-PVA, and 1000 kDa DNA-CTMA.

Polymer Name	Bias Voltage (V)	Temperature ($^{\circ}C$)	Relative Dielectric Constant	Loss Tangent at 15 GHz
DNA-CTMA	0	25	6.2855	0.2721
DNA-CTMA	0	100	5.7671	0.1789
DNA-CTMA	20	25	5.4606	0.3282
DNA-CTMA	20	100	5.8394	0.1899
APC	0	25	4.8591	0.2436
APC	0	100	4.7473	0.1693
APC	20	25	4.8439	0.2731
APC	20	100	4.7473	0.1693
BSA-PVA	0	25	6.5019	0.3138
BSA-PVA	0	100	6.9456	0.2639
BSA-PVA	20	25	5.7863	0.3477
BSA-PVA	20	100	5.8783	0.2735
PVA	0	25	5.0208	0.1288
PVA	0	100	5.6210	0.1823
PVA	20	25	5.0414	0.1542
PVA	20	100	5.3348	0.2241

used in this study. Both biopolymers have higher loss tangents than the reference polymers at room temperature, and the loss tangent of BSA-PVA is always higher than that of PVA. Therefore, adding biologically-based materials to a polymer, as is done to make BSA-PVA, can increase both the relative dielectric constant and loss tangent of the material. The mean relative dielectric constant decreases with increasing voltage at room temperature for both biopolymers, while it stays the same in APC and increases slightly in PVA. At 100 °C, the mean relative dielectric constant decreases in both PVA and BSA-PVA. With no applied bias and increasing temperature, the mean relative dielectric constant decreases in DNA-CTMA and APC, and increases in BSA-PVA and PVA. With 20.0 V applied bias and increasing temperature, the mean relative dielectric constant increases for both PVA and BSA-PVA. The mean loss tangent at 15 GHz decreases with increasing temperature for both biopolymers, while in PVA the mean loss tangent increases with increasing temperature. These observations show that while sometimes a biopolymer made from a known polymer material will have the same properties as the known polymer material, that is not always the case. These trends show that the electrical characteristics of all biopolymers, even those made from well-known polymers need to be studied before they can be successfully used in electronic devices.

To help identify electronic applications, where these biopolymer thin films might be useful, it is necessary to identify how each individual material responds to changes in applied voltage and temperature. These individual responses, in conjunction with comparisons to the response of APC, help focus further studies and identify applications in which these new biopolymer thin films can be used. The following subsections focus on identifying and analyzing the response of each of the polymers and biopolymers studied under the various conditions measured. The dielectric properties of the biopolymers are also compared to the response of a known ferroelectric material, barium strontium titanate (BST).

4.3.1 APC

A typical example of S21 data obtained for the reference polymer, APC, is plotted in Figure 4.6. This figure shows that at room temperature the value of S21 decreases with increasing frequency, and at 100 °C the value of S21 decreases with increasing frequency for frequencies above 6.4 GHz, while at frequencies below 6.4 GHz there is a brief decrease in S21 and then an increase. These lower frequency, high temperature effects on S21 are probably caused by the conductor thickness and skin depth effects occurring at slightly higher frequencies than expected, and therefore the brief increase in S21 at 100 °C should be neglected. From Figure 4.6 it is evident that changing the bias voltage applied to APC in the capacitive test structure does not affect its frequency response. Also

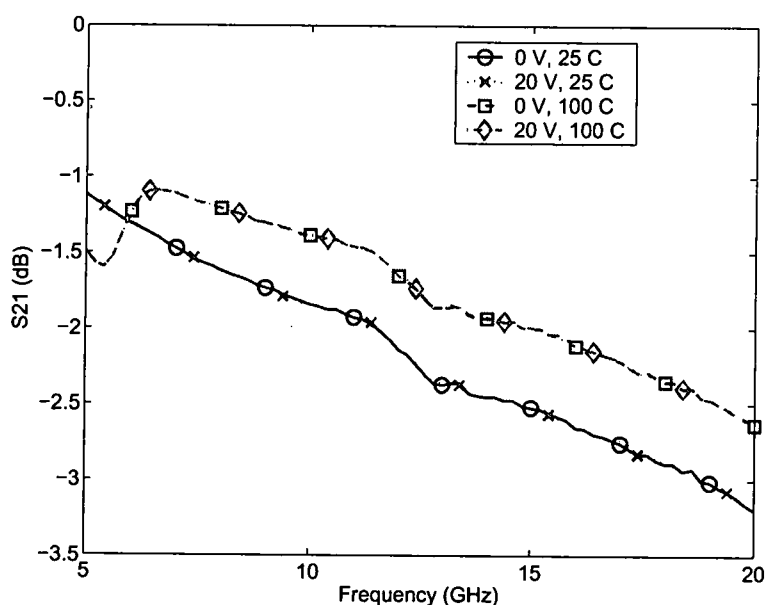


Figure 4.6: The frequency response of S21 for a capacitive test structure of APC.

note that increasing the temperature of the polymer increases the transmittance of the signal for frequencies above seven gigahertz.

4.3.2 PVA

The frequency dependence of S_{21} obtained from a capacitive test structure containing PVA is plotted in Figure 4.7. This figure shows that the transmittance of PVA decreases monotonically with increasing frequency at both room temperature and 100 °C. The room temperature transmittance is higher than the transmittance at 100 °C for PVA. From Figure 4.7 it is evident that changing the bias voltage applied to PVA does not cause a significant change in the frequency response over the frequency range of one to twenty gigahertz.

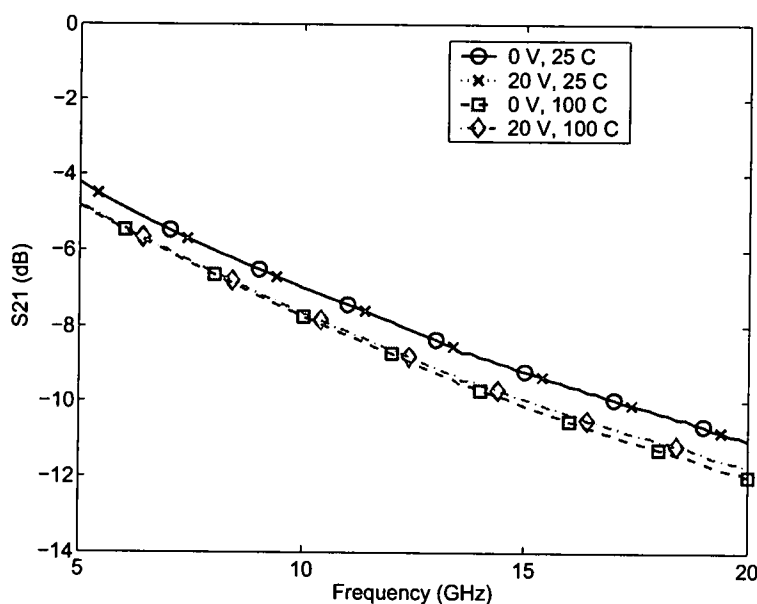


Figure 4.7: The frequency response of S_{21} for a capacitive test structure containing PVA.

4.3.3 BSA-PVA

The frequency response of S_{21} for the BSA-PVA thin film at room temperature is plotted in Figure 4.8. This figure shows that the value of S_{21} decreases with increasing frequency for all applied voltages within the frequency range of five to twenty gigahertz. The decrease seen in the transmittance over the entire frequency range is reduced as the applied voltage increases from 0.0 to 20.0 V. There is no obvious change in S_{21} values as the applied voltage changes from 0.0 to 10.0 V. As the applied voltage changes from 10.0 to 15.0 V there is a slight increase in the transmittance values. From 15.0 to 17.5 V the largest increase in transmittance occurs, and from 17.5 to 20.0 V the transmittance values also increase substantially.

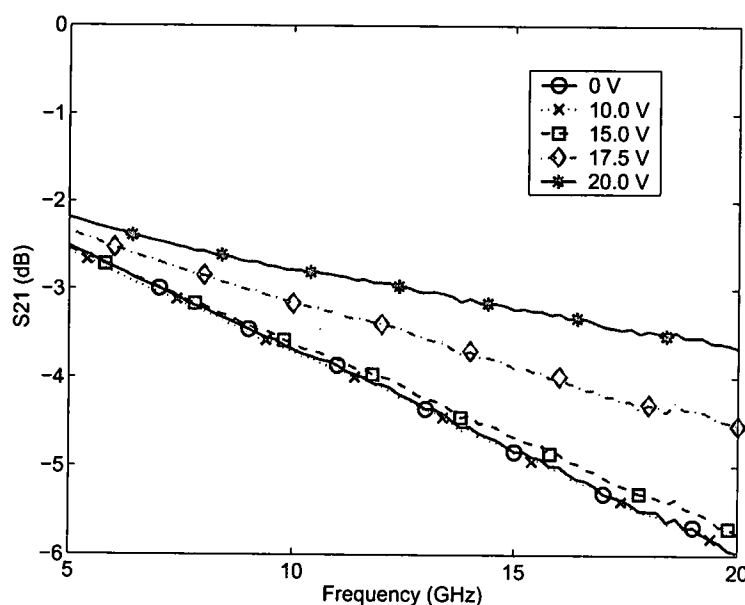


Figure 4.8: The frequency response of S_{21} for a capacitive test structure containing BSA-PVA for various applied biases from 0 to 20 V.

This change in transmittance corresponds to a decrease in the equivalent circuit capacitance and also in the relative dielectric constant of BSA-PVA. Figure 4.9 shows the calculated relative dielectric constant of BSA-PVA as a function of the applied voltage obtained from analyzing the S parameters measured from a capacitive test structure containing BSA-PVA at room temperature. This figure shows that the relative dielectric constant decreases with increasing applied bias above 12.5 V. The specific applied biases where dielectric tuning begins and where the change in relative dielectric constant is greatest are easier to identify in Figure 4.9 than they are in Figure 4.8, because the dielectric tuning corresponds directly to the slope of the curve in Figure 4.9. When the slope is zero, the relative dielectric constant is a constant value over the frequency range, and when the slope is non-zero, the relative dielectric constant is changing with applied voltage. The change in

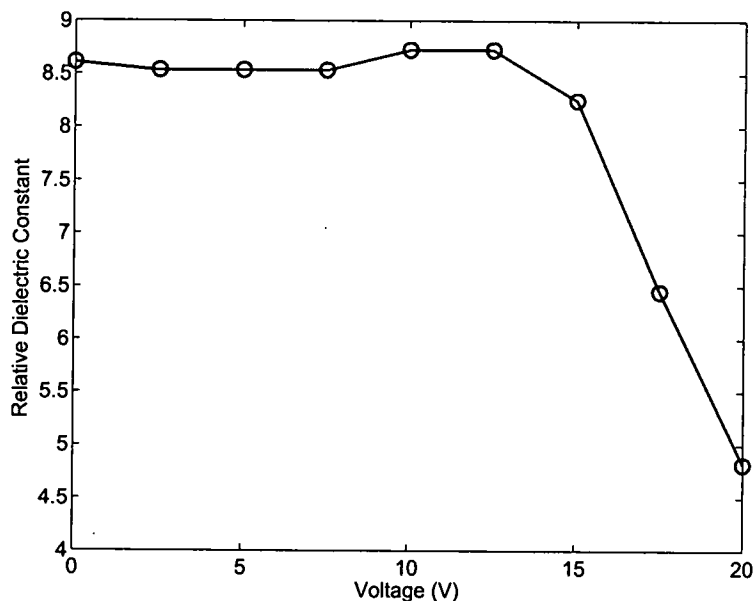


Figure 4.9: The calculated relative dielectric constant as a function of applied voltage for BSA-PVA using the measured S parameters from a capacitive test structure at room temperature.

relative dielectric constant is greatest when the slope is steepest. The relative dielectric constant of the room temperature BSA-PVA film is 8.61 at 0.0 V and drops to a value of 4.82 at 20.0 V. The percent tuning is calculated as

$$\% \text{ tuning} = \frac{\epsilon_r(0) - \epsilon_r(V_1)}{\epsilon_r(0)} \times 100 \quad (4.8)$$

where $\epsilon_r(0)$ is the relative dielectric constant with no applied bias and $\epsilon_r(V_1)$ is the relative dielectric constant with an applied bias of V_1 applied. Using this equation and the relative dielectric constant values at 0.0 and 20.0 V, BSA-PVA tunes by 44% as the applied electric field changes from 0 to 86 kV/cm.

To quantify if the measured tuning is statistically significant, a two-sided paired t-test is used to determine if there is a difference in the relative dielectric constant values for the BSA-PVA film at 0.0 and 20.0 V. Using the paired t-test, $|t| = 1.82$, which is greater than $t_{0.05} = 1.782$. Therefore, it can be concluded at the 90% confidence level that there is a difference in the relative dielectric constants of the BSA-PVA film at 0.0 and 20.0 V.

The frequency response of S21 for the BSA-PVA thin film at 100 °C is plotted in Figure 4.10. This figure shows that the value of S21 decreases with increasing frequency, over the entire frequency range, for all applied voltages. The decrease in the transmittance is seen over the frequency range of five to twenty gigahertz for all applied voltages. There is no obvious change from 0.0 to 5.0 V. The largest increase in transmittance occurs between 5.0 and 7.5 V. Another large increase in transmittance takes place from 7.5 to 10.0 V. The transmittance remains mostly constant from 10.0 to 15.0 V, and then decreases slightly from 15.0 to 20.0 V.

Again, the change in transmittance corresponds to a decrease in the equivalent circuit capacitance and the relative dielectric constant of BSA-PVA at 100 °C. Figure 4.11 shows the calculated

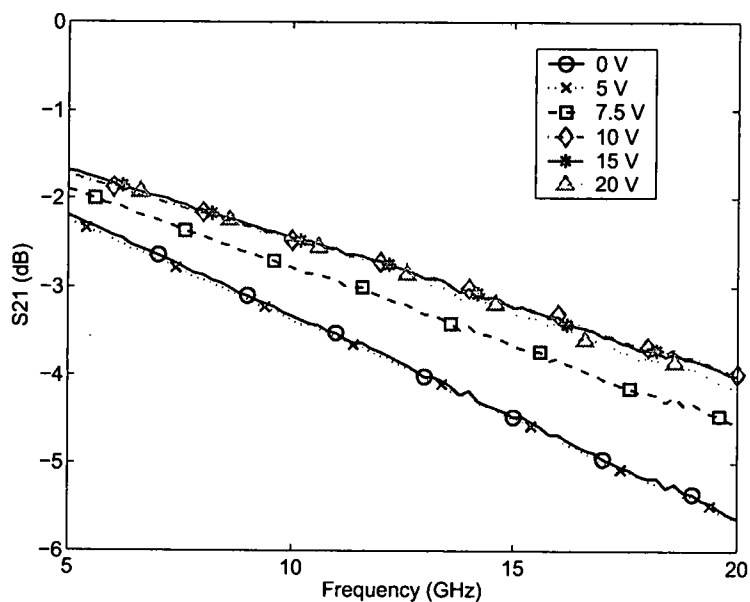


Figure 4.10: The frequency response of S21 for a capacitive test structure containing BSA-PVA at 100 C for various applied biases from 0 to 20 V.

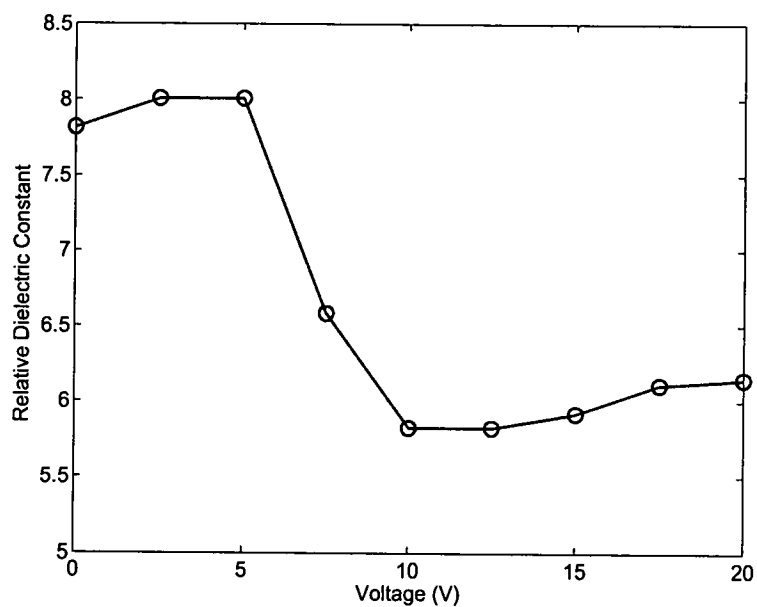


Figure 4.11: The calculated relative dielectric constant as a function of applied voltage for BSA-PVA using the measured S parameters from a capacitive test structure at 100 C.

relative dielectric constant of BSA-PVA as a function of the applied voltage obtained from analyzing the S parameters shown in Figure 4.10. The relative dielectric constant of the 100 °C BSA-PVA film is 7.82 at 0.0 V and drops to a value of 6.15 at 20.0 V. This corresponds to 21% dielectric tuning as the applied electric field changes from 0 to 86 kV/cm. Figure 4.11 shows that the relative dielectric constant increases slightly with increasing applied bias up to about 5.0 V, then decreases rapidly with increasing applied bias to 10.0 V, and again increases slightly above 10.0 V. The significant tuning takes place between 5.0 V, where the relative dielectric constant is 8.0, and 10.0 V, where the relative dielectric constant drops to a value of 5.83. Therefore, the relative dielectric constant of the BSA-PVA film at 100 °C changes by 27% as the applied electric field changes from 21 to 43 kV/cm.

Once again, to quantify if the tuning is statistically significant, a two-sided paired t-test is used to determine if there is a difference in the relative dielectric constant values for the 100 °C BSA-PVA film at 0.0 and 20.0 V. Using the paired t-test, $|t| = 2.23$, which is greater than $t_{0.05} = 2.132$. Therefore, it can be concluded at the 90% confidence level that there is a difference in the relative dielectric constants of the 100 °C BSA-PVA film at 0.0 and 20.0 V.

The BSA-PVA sample consists of numerous capacitive test structures, and the measurements on this sample are taken at two different times. The majority of the reported measurements are taken over the course of a year immediately following the sample fabrication. Then, the sample is stored in a room temperature vacuum storage oven for a year. At the end of the year, additional measurements are taken. The measurements taken after storage of the sample yield some additional interesting results. One of these results is that BSA-PVA shows hysteresis or memory effects. After increasing the bias voltage on the sample from 0 to 20 V and noticing tuning, returning the voltage to a lower voltage did not return the transmission values to their original values. In fact, taking the

applied bias from 0.0 to 20.0 V in 5.0 V steps and then returning to 10.0 V, where the transmission curves begin to tune, the second measurement at 10.0 V yielded a slightly higher transmission than the 20.0 V applied bias. This confirms analysis described in a personal correspondence with Dr. Lawrence Brott that the BSA-PVA material has some memory. Additionally, after taking data on a single test structure on the BSA-PVA thin film sample with various bias voltages at room temperature, a visual examination of the capacitive test structure yields obvious changes in the thin film near the active region. This implies that having an applied bias on the BSA-PVA sample for an extended period of time may cause changes to occur in the thin film. Finally, after taking data with a large variety of bias voltages at 100 °C, the BSA-PVA sample is returned to room temperature. After the return to room temperature, all of the capacitive test structures show a spike in current with an applied bias voltage of at most 5.0 V. This might be caused by a change in the polymer after an extended period of time at 100 °C.

4.3.4 DNA-CTMA

The frequency dependence of S21 for a capacitive test structure containing DNA-CTMA is plotted at room temperature with various applied bias voltages in Figure 4.12. This figure shows that for all applied biases measured, the transmittance decreases monotonically with increasing frequency. Figure 4.12 also shows that the transmittance of the capacitive test structure containing DNA-CTMA changes with applied bias. The transmittance is constant for applied biases up to 10.0 V. At 12.5 V, the transmittance increases slightly, with a greater increase taking place at 15.0 V. The largest increase in transmittance occurs between 15.0 and 17.5 V, and the increase in transmittance is again very slight between 17.5 and 20.0 V.

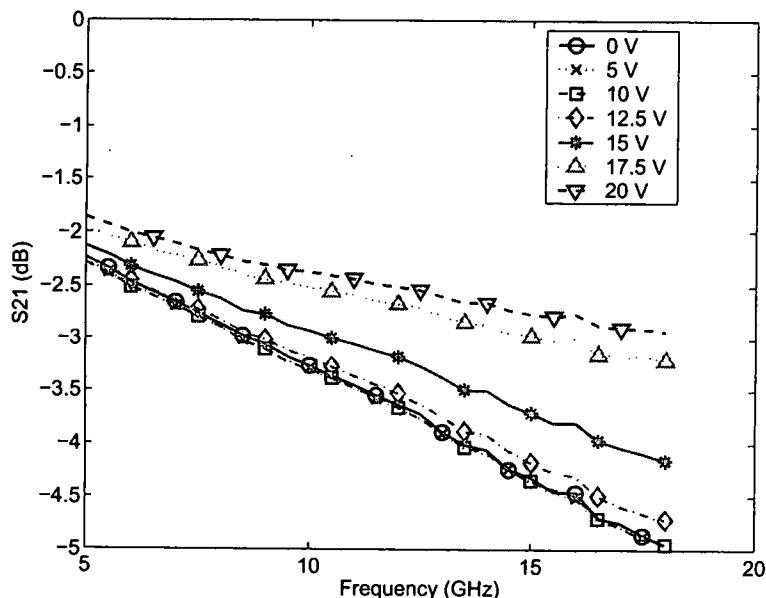


Figure 4.12: The frequency response of S21 for a capacitive test structure containing DNA-CTMA at room temperature for various applied biases from 0 to 20 V.

This change in transmittance corresponds to a decrease in the equivalent circuit capacitance and also in the relative dielectric constant of the DNA-CTMA. Figure 4.13 shows the calculated relative dielectric constant of DNA-CTMA as a function of applied voltage obtained from analyzing the S parameters in Figure 4.12 measured on a capacitive test structure containing DNA-CTMA. This figure shows that the relative dielectric constant decreases with increasing applied bias. When the slope is zero, the relative dielectric constant is a constant value. When the slope is non-zero, the relative dielectric constant is changing with applied voltage. The change in relative dielectric constant is greatest when the slope is steepest. The relative dielectric constant of the DNA-CTMA film is 6.56 at 0.0 V and drops to a value of 3.12 at 20.0 V. This corresponds to 52% dielectric tuning as the applied electric field changes from 0 to 113 kV/cm.

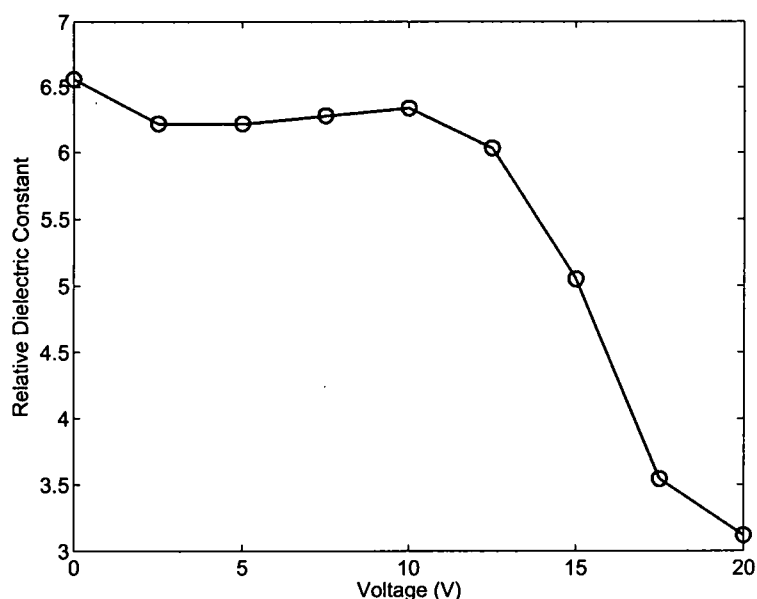


Figure 4.13: The calculated relative dielectric constant as a function of applied voltage for DNA-CTMA using the measured S parameters from a capacitive test structure.

To quantify if the measured tuning is statistically significant, a two-sided paired t-test is used to determine if there is a difference in the relative dielectric constant values for the DNA-CTMA film at 0.0 and 20.0 V. Using the paired t-test, $|t| = 2.15$, which is greater than $t_{0.05} = 1.80$. Therefore, it can be concluded at the 90% confidence level that there is a difference in the relative dielectric constants of the DNA-CTMA film at 0.0 and 20.0 V. These results from the two-sided paired t-test provide confidence in the analysis that the DNA-CTMA film tunes with applied voltage.

Figure 4.14 shows the frequency response of S21 for a capacitive test structure containing DNA-CTMA at 100 °C with various applied biases. This figure shows that the transmittance decreases with increasing frequency for both 0 and 20 V at 100 °C. Figure 4.14 also shows that S21 does

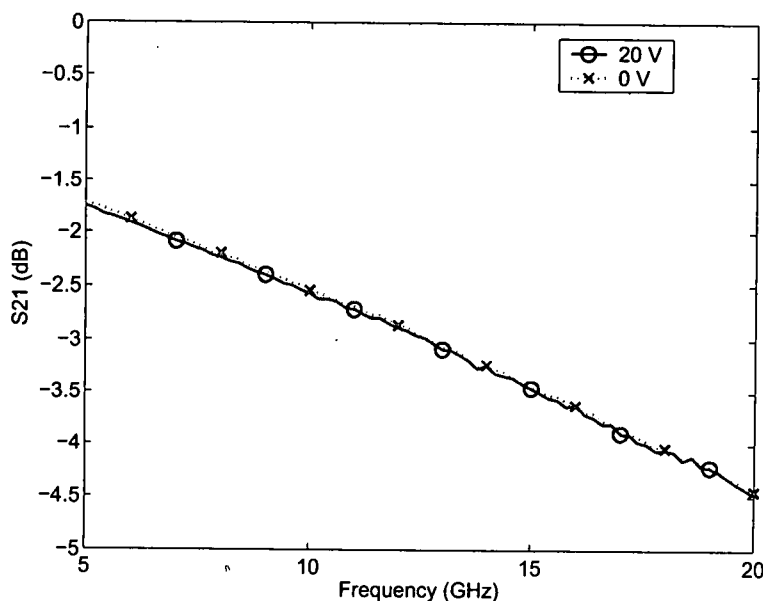


Figure 4.14: The frequency response of S21 for a capacitive test structure containing DNA-CTMA at 100 °C for various applied biases from 0 to 20 V.

not change with applied bias for DNA-CTMA at 100 °C. This means that while the relative dielectric constant of DNA-CTMA tunes at room temperature, as the temperature increases it does not continue to tune. The reason why the dielectric tunability is present at room temperature but not at 100 °C is unknown. One possible explanation, however, is that the thin film of DNA-CTMA has a glass transition temperature, T_g , between room temperature and 100 °C. The T_g of DNA-CTMA thin films is unknown because it is undetectable by differential scanning calorimetry, although the T_g of the DNA-CTMA powder has been measured to be 148 °C [89]. If the DNA-CTMA thin film has passed the transition temperature by 100 °C, then the DNA-CTMA thin film is softer and more flexible at 100 °C than it is at room temperature. This change might explain the differences in the transmittance measurements at room temperature and 100 °C for this biopolymer.

4.3.5 BST

The dielectric properties of the tunable biopolymers described above should be compared to a known inorganic material with voltage tunable dielectric properties, such as barium strontium titanate (BST). The frequency response of S21 for a capacitive test structure containing 300 nm of BST is plotted in Figure 4.15 with applied biases varying from 0.0 to 3.0 V. This figure shows that the transmittance decreases with increasing frequency at each of these applied biases. The figure also shows that the transmittance increases with increasing applied bias, and confirms that the dielectric properties of BST tune with applied bias. The increasing transmittance corresponds to a decreasing capacitance and therefore a decreasing relative dielectric constant. The relative dielectric constant tunes by 47% as the applied voltage changes from 0.0 to 3.0 V, which for the 300 nm thick film of BST corresponds to a change in the applied electric field from 0 to 100 kV/cm at room temperature.

It is useful to note that the BSA-PVA film tunes slightly less than the BST at room temperature, while the DNA-CTMA film tunes more than the BST film at room temperature. Both the DNA-CTMA and BSA-PVA films are unoptimized and are already showing tuning on the order of that seen in the BST film. This suggests that the biopolymers can be used in applications that utilize dielectric tunability, such as sensors and antennas.

4.4 Capacitance Measurements

Capacitance is measured as a function of frequency to confirm that the electrical properties obtained from the microwave measurements are those of the polymer. This can be done by showing that the capacitance in the electrical model is that of the polymer and is not due to interface charges.

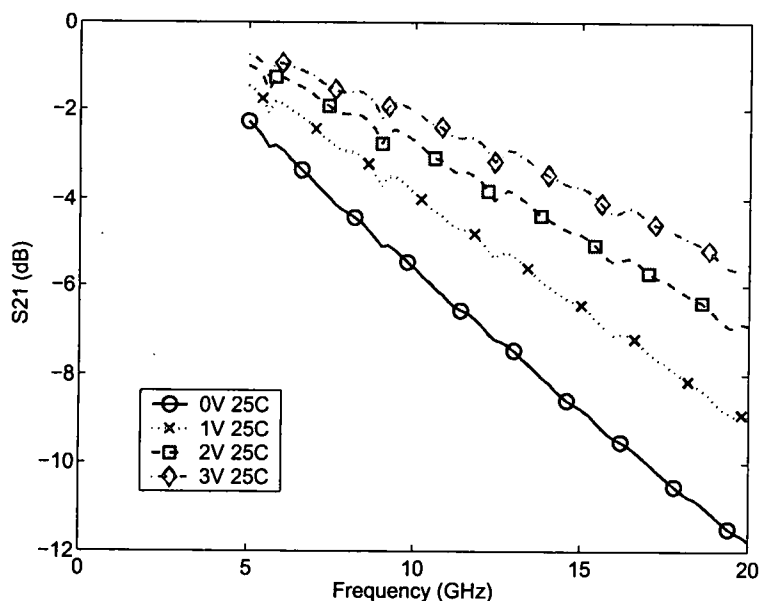


Figure 4.15: The frequency response of S21 for a capacitive test structure containing BST for applied biases from 0 to 3 V.

An on-wafer probe station with micromanipulators and a HP 4284A Precision LCR (inductance-capacitance-resistance) meter are used to perform low-frequency characterization on thin films using the capacitive test structure. The LCR meter has the ability to vary the voltage, from -40 V to 40 V, and the frequency, from 20 Hz to 1 MHz, and to measure current. Using this equipment, the capacitance and dissipation factors can be obtained as a function of either frequency or bias voltage.

One example of the low frequency capacitance measurements obtained as a function of frequency for a DNA-CTMA capacitive test structure is plotted in Figure 4.16. This figure shows that the capacitance is very high at low frequencies and decreases to the bulk capacitance with increasing frequency. The high capacitance present at very low frequencies is due to interface charges that are quickly depleted as the frequency increases. The rate of depletion slows down as the frequency

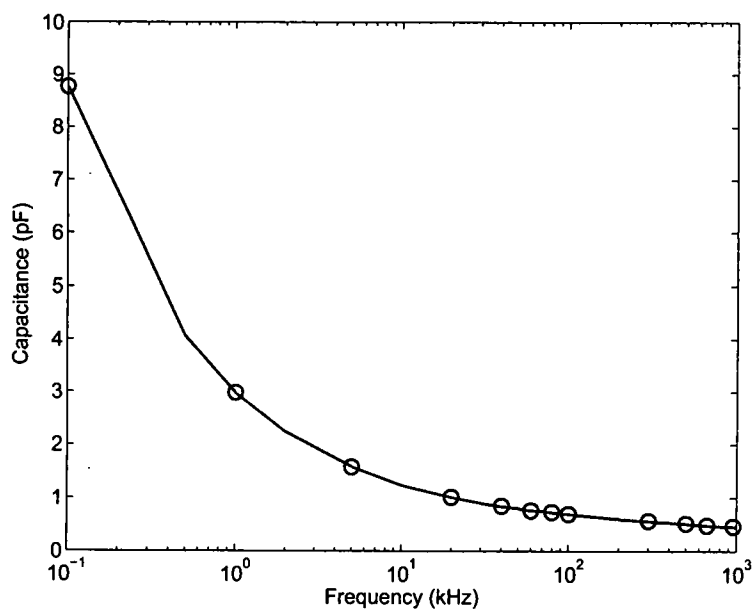


Figure 4.16: Capacitance as a function of frequency on a log scale for one capacitive test structure made with a DNA-CTMA thin film.

increases and therefore equilibrium is approached at the higher frequency values. The equilibrium capacitance value is that of the bulk capacitance and is the same as that obtained from the microwave frequency measurements. Other capacitive test structures have been measured in this same manner and produce similar results. This verifies that the capacitance values, and therefore the relative dielectric constant and loss tangents obtained from the microwave characterization measurements described above, are for the bulk polymer and are not due to the polymer-metal interfaces in the capacitive test structure.

4.5 Electric Force Microscopy

Electric force microscopy (EFM) images are taken to examine the mechanisms of the dielectric tunability observed for the capacitive test structure containing DNA-CTMA. These measurements map the surface topography of the test structure and show the effect of a constant DC bias applied to the DNA-CTMA film by measuring the change in the electric field gradient across the region of interest. Changing the applied DC bias will confirm the dielectric tunability, if large changes in the EFM images are observed.

Atomic force microscopy (AFM) produces high resolution images of the surface topography. To obtain these topography images, a sharp tip on the edge of a flexible cantilever is scanned across the surface of the sample while the system maintains a small and constant force between the sample and the tip. The tip scans the surface in a raster pattern. The deflection of the tip is detected by a laser beam reflecting off the back of the cantilever into a photodetector, where differences in the output voltage correspond to changes in the cantilever deflection [94].

In this research, TappingMode AFM is used, in conjunction with EFM and Phase Imaging using a Veeco Instruments MultiMode Scanning Probe Microscope equipped with a NanoScope IIIa Controller and Quadrex Phase-Detection [95]. TappingMode AFM refers to the mode of operation where the AFM tip alternately touches the surface to make high resolution images and is lifted off of the surface to move between imaging locations, to avoid damaging the surface of the sample. In this mode, the AFM cantilever oscillates at its resonance frequency to lightly tap the surface with the AFM tip while imaging. The deflection of the laser beam is used to keep the tip a constant distance from the sample by moving the scanner vertically at every data point. The topographical image of the surface is formed from a record of the scanner's movement.

EFM maps the gradient of the electric field present between the tip and the sample at every point. The EFM images are generated by plotting the change in the phase, frequency, or amplitude of the cantilever oscillation as it encounters vertical repulsive and attractive electric field forces above the sample surface at each point [96]. The change in phase or frequency detection are more commonly used than amplitude detection, as these methods result in better images. A DC bias voltage is applied to the sample through a conductive platinum-iridium coated AFM tip. The field variations due to trapped charges are mapped using EFM. This study images the electric field present between the sample and AFM tip by phase detection, and relies on the vertical force gradients from the sample causing changes in the resonance frequency of the cantilever. Attractive forces cause the AFM tip to be closer to the sample, thereby reducing the resonance frequency and increasing the phase component of the oscillating cantilever EFM.

Phase Imaging maps the phase of the cantilever oscillations during TappingMode AFM scans. The phase lag of the cantilever, with respect to the drive signal, is monitored for each point during the scan. This imaging highlights edges and provides more information about fine features that can be hidden by a rough surface [97].

The scans are performed on a five micron square area of the center of a capacitive test structure containing DNA-CTMA in air at ambient temperatures. A scan rate of two Hertz is used with cantilever resonance frequencies of 65 to 68 kHz. Silver paint is applied from the steel magnetic AFM sample stub to the top of the grounding pads to provide a consistent ground. LiftMode is used to obtain the EFM maps of electric field gradient and distribution as a function of applied voltage, ranging from 0.0 to 12.0 V. LiftMode separately measures topography and electric force in a two pass technique, using topographic information to track the probe tip at 41 nm above the surface.

Figures 4.17 and 4.18 show the TappingMode topography, EFM, and phase images from left to right, as measured on the active region of the capacitive test structure, with applied DC biases of 5.5 V, 6.0 V, 6.5 V, 7.0 V, and 7.5 V. The phase component of the electric field is mapped in the center images and shows a dramatic increase in the phase of the electric field from 5.5 to 7.0 V, and then decreases from 7.0 to 7.5 V. As the bias applied to the AFM tip increases from 5.5 to 7.0 V, the EFM images show that the phase increases. This increase in phase is due to an increase in the attractive force between the sample and the AFM tip that causes the resonant frequency to

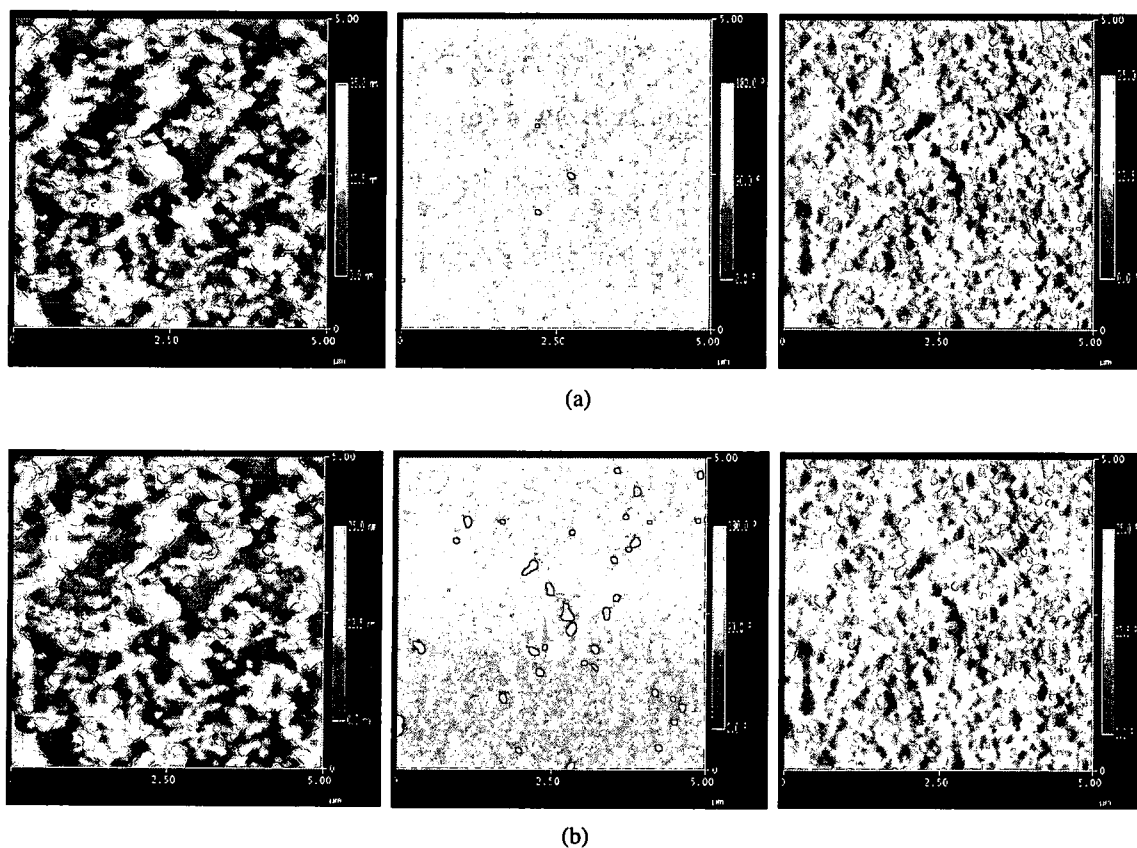


Figure 4.17: TappingMode Topography (left), Electric Force Microscopy (center) and Phase Images (right) with DC biases of (a) 5.5 V and (b) 6.0 V applied to the AFM tip. The phase component of the Electric Field is observed over a 5 micron x 5 micron region in the center of the image.

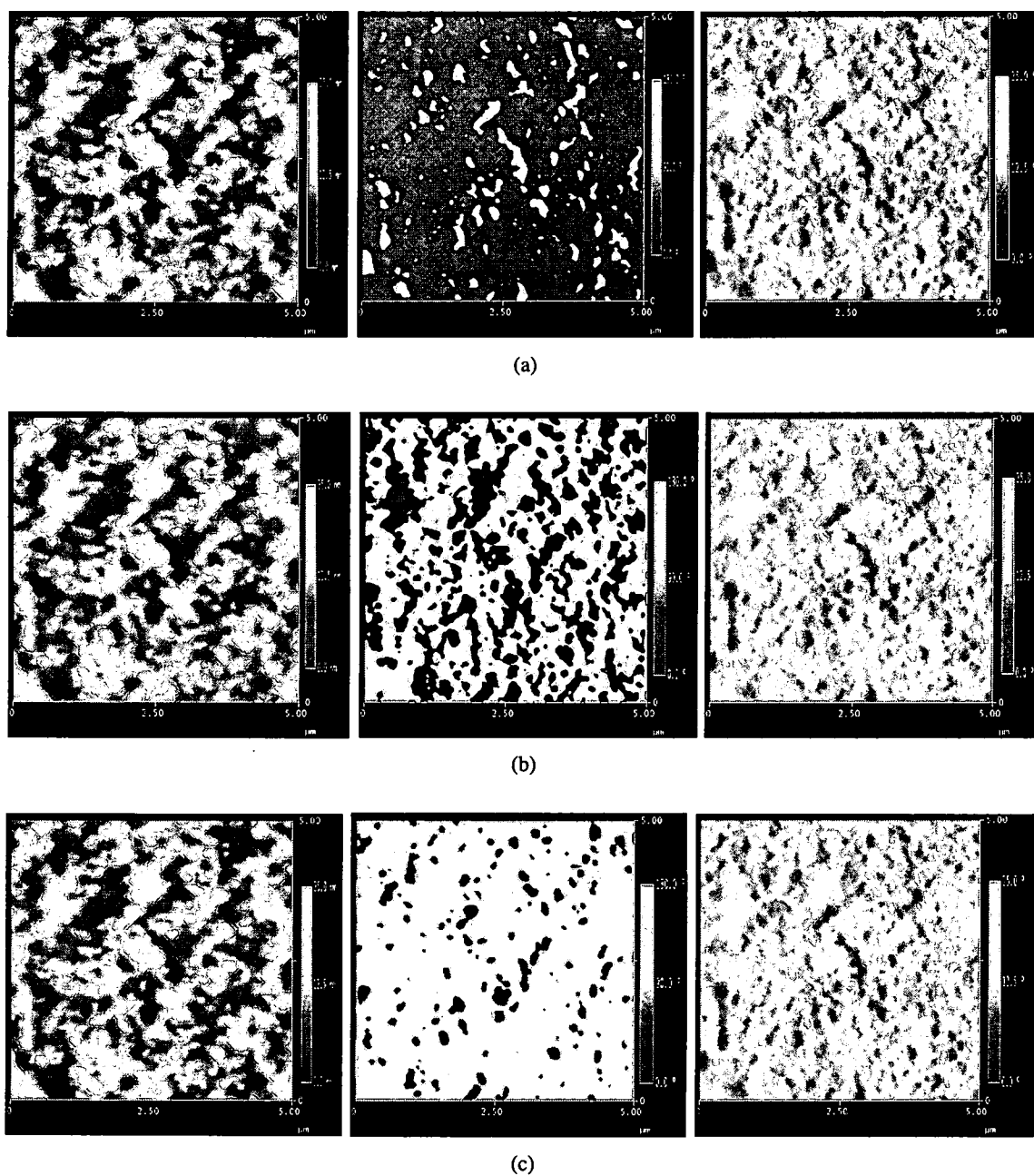


Figure 4.18: TappingMode Topography (left), Electric Force Microscopy (center) and Phase Images (right) with DC biases of (a) 6.5 V, (b) 7.0 V and (c) 7.5 V applied to the AFM tip. The phase component of the Electric Field is observed over a 5 micron x 5 micron region in the center of the image.

decrease. As the voltage on the AFM tip increases from 7.0 to 7.5 V, the EFM images show that the phase decreases, which corresponds to an increase in the resonant frequency of the AFM tip. This change in the direction of the phase is caused by a change in the effective dipole moment in the DNA-CTMA layer which is seen as a decrease in the relative dielectric constant in the original S parameter measurements on the capacitive test structure made with the DNA-CTMA thin film.

4.6 Summary

This chapter describes a new capacitive test structure that is used to characterize the dielectric properties of polymer and biopolymer thin films. The use of this capacitive test structure shows that the biopolymers BSA-PVA and DNA-CTMA have dielectric properties that tune with applied bias, while the reference polymers APC and PVA do not tune with applied bias. The BSA-PVA is seen to tune at both room temperature and 100 °C, while the DNA-CTMA only tunes at room temperature. The DNA-CTMA film without any optimization tunes more than the BST film. The dielectric tunability of DNA-CTMA is further studied in this chapter by EFM images and capacitance measurements. The capacitance measurements show that interface charges only affect the capacitance measurements at low frequencies, and at high frequencies the measured capacitance is that of the bulk capacitance. This verifies that the microwave characterization does indeed provide bulk material properties because the capacitance obtained from the S parameter data is that of the bulk capacitance. The EFM images verify that the electric field response of the DNA-CTMA thin film changes with applied field.

The next chapter describes the development of the first polymer transistor to use a DNA-biopolymer as the semiconductor material. Several structures will be examined, and the data measured from these will be described. Problems encountered will be explained with possible solutions

presented. Finally, a DNA-biopolymer based transistor will be presented, the current-voltage curves shown, and transistor parameters calculated.

CHAPTER V

DNA-BIOPOLYMER SEMICONDUCTOR DEVICES

This chapter describes the development of the first field effect transistor to demonstrate the use of a DNA-biopolymer as the semiconducting layer. All the structures used in this development contain a DNA-biopolymer serving as the semiconducting layer of a biologically-based field effect transistor (BioFET). First, a brief description of the measurement system used throughout the work in this chapter is given. Next, the top gate BioFET structure using DNA-biopolymers as the semiconducting layer is described, and the results obtained are presented and discussed. Third, a bottom gate BioFET structure is described and the results are presented. Finally, the results from the first DNA-based semiconducting layer in a transistor are analyzed and discussed.

5.1 Measurement setup

A Keithley 4200 Semiconductor Characterization System is connected to the transistor under study using an on-wafer micromanipulator needle probe station, shown in Figure 5.1. The semiconductor characterization system controls and measures the currents and voltages in all the transistor structures described in this chapter. This semiconductor characterization system has a current compliance level that can be set for each terminal. The current compliance level is a limit set on the measured current level that limits the power that can be delivered to the device. Using this characterization system, contact is made to the source, drain, and gate by direct contact with needle probes,

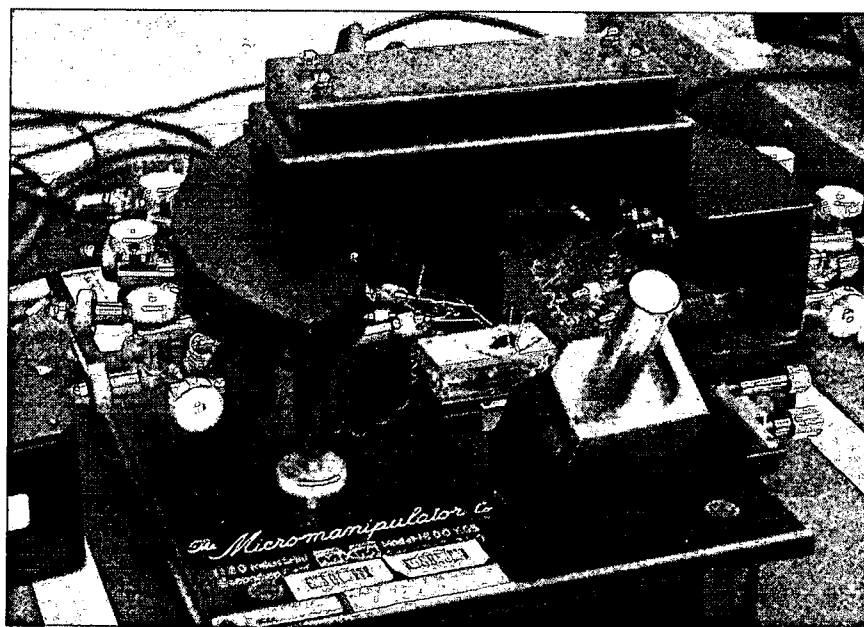


Figure 5.1: The probe station setup used for measuring the DNA-based transistors.

except when the gate is located on the bottom of the substrate. The sample holder on the needle probe station is gold coated and is therefore conductive, so when the gate is on the bottom of the substrate, the needle probe to the gate is placed directly on the sample holder rather than contacting the gate directly. The body on the top gate transistor structure is contacted in the same way as the gate on the bottom gate structure. The semiconductor characterization system is setup to function as a curve tracer, measuring, recording, and plotting current-voltage (I-V) curves for the BioFETs while also producing a spreadsheet that contains all the voltages and currents being controlled and measured during the test scan.

5.2 Top Gate BioFET Structure

The top gate DNA-based BioFETs are fabricated on a glass slide covered with a layer of indium tin oxide (ITO). The ITO serves as the body contact of the BioFET. The glass slide is oriented upside-down so that the device is fabricated on the glass side of the ITO-coated glass. This prevents the metal layers from shorting to the ITO through the spin-coated polymers while still providing a body contact. On the glass side of the ITO-coated glass, a one to two micron thin film of the DNA-biopolymer is deposited by spin-coating to form the semiconducting layer. On top of the DNA-biopolymer, the source and drain are deposited by sputtering 1000 Å of gold through a shadow mask, forming a 4.0 mm long and 10.16 mm wide channel. Then, a half micron thin film of APC (amorphous polycarbonate) is deposited by spin-coating to serve as the gate insulator. On top of the gate insulator, the gate is formed by sputtering another 1000 Å of gold through a second shadow mask. Finally, the APC deposited on top of the contact pads attached to the source and drain is removed by applying a thin layer of cyclopentanone to those areas. The complete structure is illustrated in Figure 5.2. A photograph of one of the top gate BioFETs containing a DNA-biopolymer as the semiconducting layer is shown in Figure 5.3.

Two different DNA-biopolymers, DNA-CTMA and DNA:PEDOT:CTMA, are used as the semiconducting layer in these new BioFETs. These devices will be referred to as DNA-CTMA-BioFETs, and DNA:PEDOT:CTMA-BioFETs. The DNA-CTMA used in these BioFETs is dissolved at 12 wt% in butanol to deposit a 1.5 μm thick semiconducting layer by spin-coating. The DNA:PEDOT:CTMA used in these BioFETs is dissolved at 10 wt% in butanol to spin-coat a one micron thick semiconducting layer.

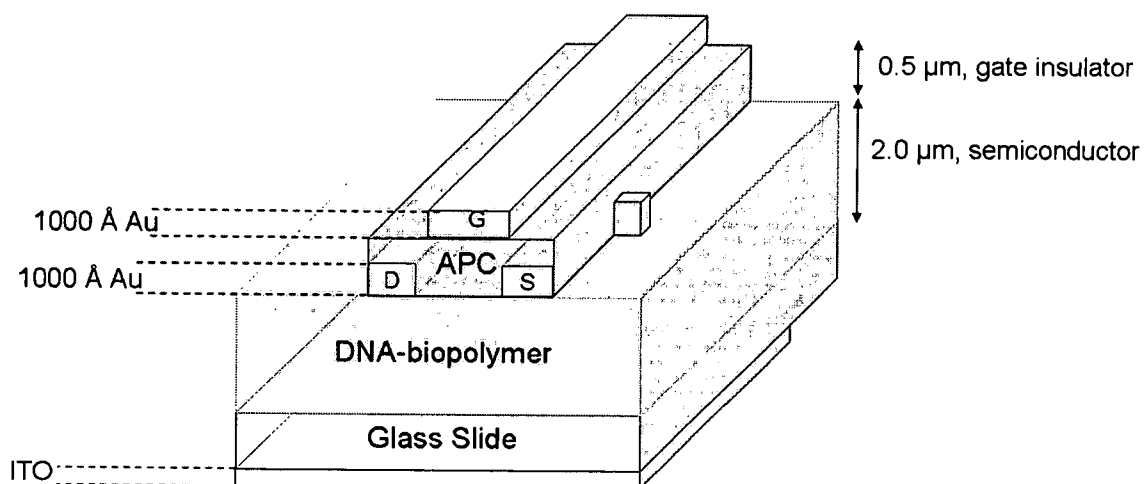


Figure 5.2: A cross-sectional view of the top-gate BioFET containing a DNA-biopolymer in the semiconducting layer.

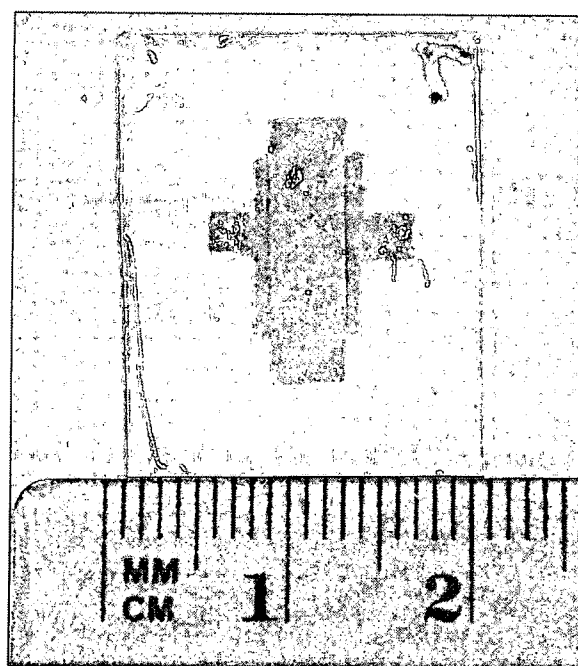


Figure 5.3: A photograph of one of the top gate BioFETs containing a DNA-biopolymer as the semiconducting layer.

5.2.1 Results with DNA-CTMA

Figure 5.4 is a plot of drain current for the DNA-CTMA-BioFET as a function of drain voltage for various gate voltages with the current compliance limit set to 100 nA on each terminal. Drain current increases nonlinearly with drain voltage for all gate voltages, as seen in this figure. The effect of gate voltage is also shown in this figure. Each curve on the plot is for a different gate voltage, and the figure shows that as gate voltage increases, the drain current decreases. For all gate voltages greater than 0.0 V, the I-V curves are the same at low drain voltages. The I-V curves separate at increasingly higher values of current and drain voltage as the gate voltage increases. At the point where a particular gate voltage curve branches off from the common current curve, the

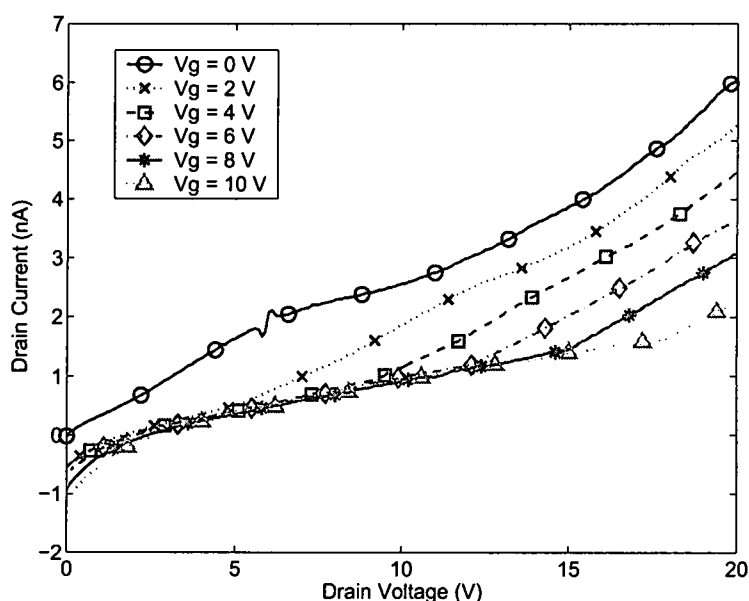


Figure 5.4: A set of current-voltage curves obtained from a transistor with DNA-CTMA used as the semiconducting layer.

drain current for that gate voltage increases more rapidly than it does for the higher gate voltage curves.

Also notice that the drain current decreases with increasing gate voltage. This indicates that the transistor is a p-channel transistor [65]. Furthermore, the gate voltage transitions from negative to positive before the drain current reaches zero. This indicates that the DNA-CTMA-BioFETs operate in depletion mode [65]. This is the first reported evidence of DNA-CTMA acting as a semiconducting material.

The DNA-CTMA-BioFET curves in Figure 5.4 resemble traditional short-channel I-V curves that have been seen in OFETs. However, according to Haddock *et al.* the ratio of channel length to insulator thickness should be less than 20 for short-channel effects to be a concern when the channel length is greater than one micron [98]. The design used for these tests have a channel length of 4.0 mm and an insulator thickness of half a micron, which produces a ratio of channel length to insulator thickness of 8000. Therefore, one would not expect short channel effects to be an issue, but further investigation is necessary to determine the reason for the resemblance to short-channel I-V curves.

5.2.2 Results with DNA:PEDOT:CTMA

Figure 5.5 is a plot of drain current for the DNA:PEDOT:CTMA-BioFET as a function of drain voltage for various gate voltages with the current compliance level set to 100 nA on each terminal. The drain current is seen to increase nonlinearly with drain voltage for gate voltages below 8.0 V. The curves corresponding to gate voltages of 8.0 and 10.0 V show no obvious increase in current for the range of drain voltages measured. As the gate voltage increases from 0.0 V, the overall drain current decreases and the I-V curves level off at progressively lower currents. This indicates that these DNA:PEDOT:CTMA-BioFETs operate in the depletion mode.

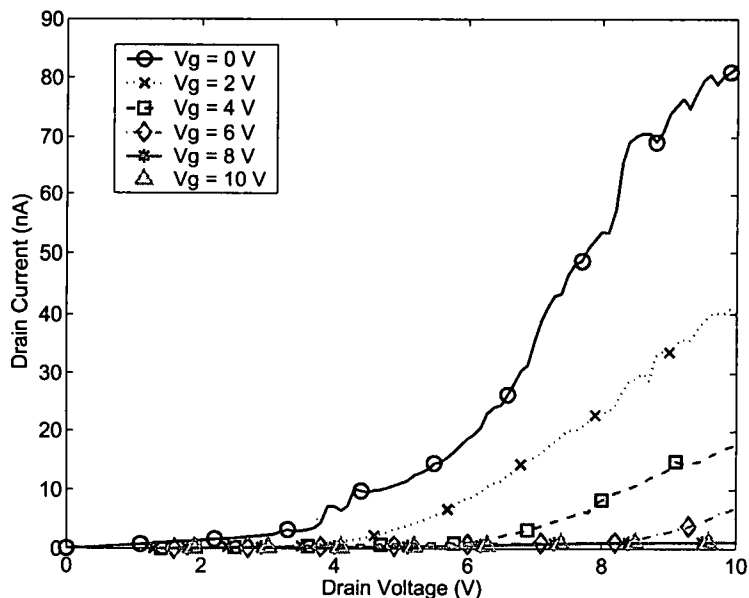


Figure 5.5: Current-voltage curves obtained from a transistor with DNA:PEDOT:CTMA used as the semiconducting layer.

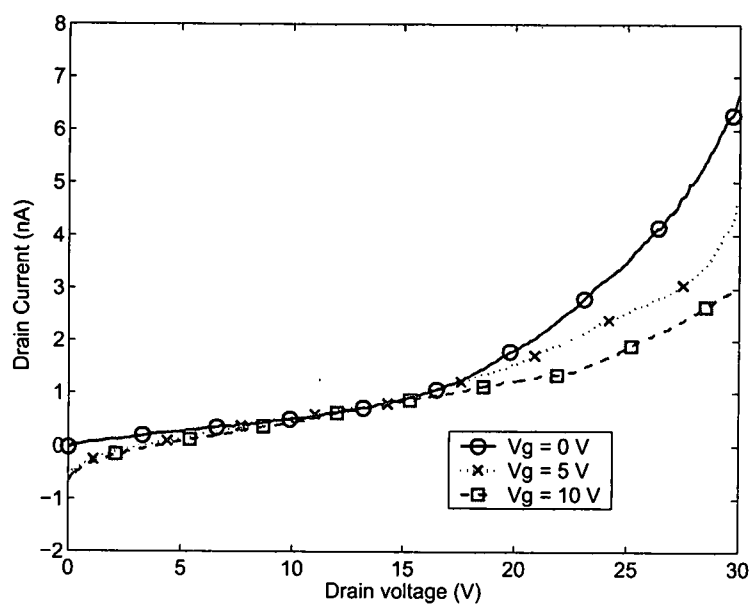
Figure 5.5 plots the first set of curves measured on the DNA:PEDOT:CTMA-BioFETs. PEDOT is a known conductive polymer, and blending it with DNA produces an overall conductivity of 10^{-3} S/cm for the complex, which is higher than the conductivity of 10^{-10} S/cm for DNA-CTMA [86]. This complex, DNA:PEDOT:CTMA, was first investigated to combine the hole transport and electron blocking layers in the BioLED. From this, determining if this material has any useful semiconducting properties was a natural next step. Based on the known improvement in conductivity in DNA:PEDOT:CTMA over DNA-CTMA, DNA:PEDOT:CTMA-BioFETs should produce higher currents at lower voltages than the DNA-CTMA-BioFETs. The high voltages at which these curves are seen is likely due to the thick layers and larger size used in these initial devices.

5.2.3 All-DNA BioFET

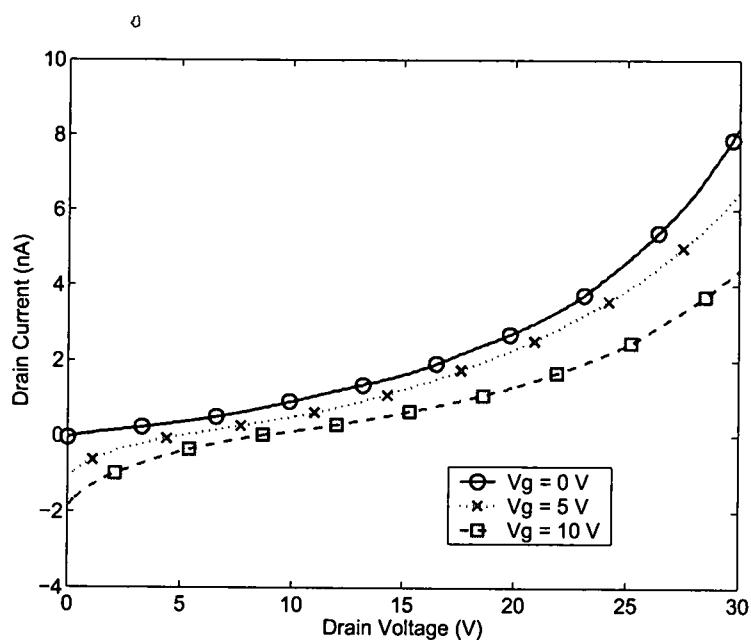
The first all-DNA BioFET of the same basic structure is also fabricated and measured. The semiconducting layer of this device is a one micron thick spin-coated layer of DNA:PEDOT:CTMA and the gate insulator is 50 nm of DNA-CTMA deposited by MBD. MBD must be used to deposit the DNA:CTMA on top of the DNA:PEDOT:CTMA because both DNA-biopolymers dissolve in the same solvents. This prevents the uniform deposition of two DNA-biopolymer films on top of each other by spin-coating, since the solvent for the second film will partially dissolve the first film producing non-uniform layers of thin films for both layers.

The I-V curves from the all-DNA BioFET are shown in Figure 5.6. This figure consists of two plots taken on the same structure with the only difference being the value of the current compliance level on the gate. The current compliance level on the gate is set to 100 nm and 200 nm, in part (a) and (b) respectively. The current compliance level set on the gate is causing the curves to clump together at low drain voltages, instead of separating out as they would do if they were unconstrained. This indicates that the gate insulator layer in the all-DNA BioFET is not acting as a good insulator.

Comparing the I-V curves for the all-DNA BioFET with the current compliance level set too low to the DNA-CTMA-BioFET and DNA:PEDOT:CTMA-BioFET curves, one finds a number of similarities. These similarities suggest that the gate currents should be examined for the DNA-CTMA-BioFET and DNA:PEDOT:CTMA-BioFET data. The gate currents for these devices are sitting at the current compliance limit when the I-V curves are clumped together and flat-lining in both cases. Therefore, gate current leakage is a real problem in this structure. However, the non-linearities seen in the measured I-V curves show promise for the use of DNA-based biopolymer thin films as semiconducting materials in transistors. DNA-CTMA has been successfully used as a



(a)



(b)

Figure 5.6: Current-voltage curves obtained from the all-DNA BioFET with current compliance set at (a) 100 nA and (b) 200 nA.

gate insulator in polymer FETs, but only when using high molecular weight DNA-CTMA [15]. The low molecular weight DNA-CTMA used here has not been reported as a successful gate insulator. The DNA-CTMA layer in the all-DNA BioFET is deposited by MBD, which is only able to deposit low molecular weight DNA-CTMA. Therefore, a better understood gate insulator needs to be used to test the DNA-based biopolymers as semiconducting layers in BioFETs. In the next section, an alternative design is used to address the high gate currents.

5.3 Bottom Gate BioFET Structure

One of the standard polymer transistor gate insulators seen in the literature is silicon dioxide used in a bottom gate FET structure. In the literature, this structure is built from low resistivity silicon wafers with a silicon dioxide layer on top of the silicon. The gate is on the unpolished side of the silicon wafer, with the silicon dioxide, SiO_2 , serving as the gate insulator. The source and drain are patterned on top of the SiO_2 , and on top of the source and drain the semiconducting polymer is deposited [67]. This structure is examined in an attempt to reduce the gate leakage current measured in the top gate BioFET structure.

As an initial attempt, a similar bottom gate BioFET structure, containing DNA:PEDOT:CTMA as the semiconductor, is fabricated using undoped silicon with the very thin layer of naturally occurring SiO_2 on the silicon wafer instead of a thicker deposited layer of SiO_2 on low resistivity silicon. Undoped silicon wafers are more readily available in the lab as these silicon wafers are used for the fabrication of the capacitive test structures described in Chapter IV. Therefore, bottom gate BioFETs containing DNA:PEDOT:CTMA are initially fabricated on undoped silicon with a thin native oxide layer to determine if further investigation of this structure is worthwhile.

The cross-section of the fabricated structure is illustrated in Figure 5.7. This structure has the

gate contact on the unpolished side of a $304.8\ \mu\text{m}$ thick undoped silicon wafer, while SiO_2 is on the polished side of the silicon wafer. The source and drain are patterned on top of the SiO_2 by sputtering $1000\ \text{\AA}$ of gold through a shadow mask, forming a $4.0\ \text{mm}$ long and $10.16\ \text{mm}$ wide channel. On top of the source and drain, a one micron thick layer of DNA:PEDOT:CTMA is applied by spin-coating to act as the semiconductor. Based on the results from the undoped silicon with a native oxide layer on it, a slightly different design for the bottom gate BioFET structure is also fabricated. This second bottom gate structure uses an undoped silicon wafer with a $500\ \text{nm}$ layer of SiO_2 deposited on the polished side of the silicon by RF sputtering, but is otherwise the same as the structure made with the native oxide dielectric layer.

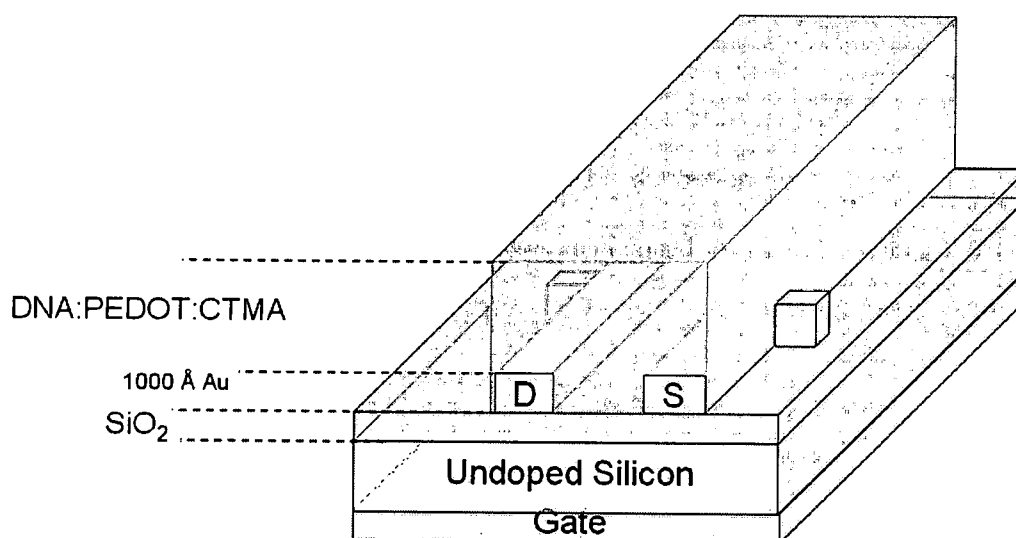


Figure 5.7: A cross-section of the bottom gate BioFET structure.

5.3.1 Results

Figure 5.8 shows a set of current-voltage curves with gate voltages varying from -20.0 to 5.0 V for a bottom gate BioFET fabricated on a silicon wafer with a very thin SiO_2 layer. The current compliance limit is set to 0.5 mA on each terminal. This plot is the first set of measured I-V characteristics to show a steep increase, followed by a linear increase with a much smaller slope. The transition between the two regions occurs at nearly the same drain voltage, about 0.5 V, for all gate voltages. As the gate voltage increases from -20.0 to 0.0 V, the drain current decreases at positive drain voltages. This response is similar to that of a transistor operating in depletion mode. Interestingly, as the gate voltage increases from 0.0 to 5.0 V, the steep increase no longer

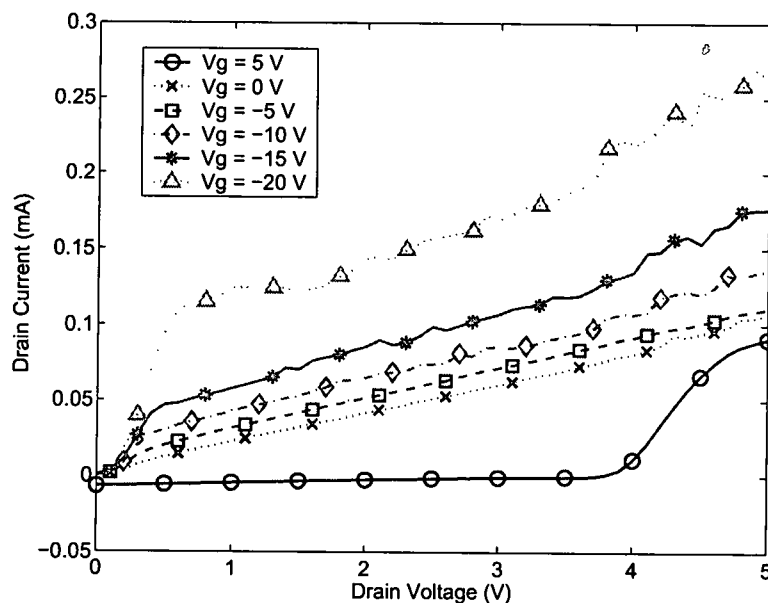


Figure 5.8: Drain current as a function of drain voltage as measured on a bottom gate BioFET fabricated on an undoped silicon wafer with a very thin silicon dioxide layer as the gate insulator, clearly showing control by the gate voltage.

takes place at 0.0 V, but instead occurs around 4.0 V. The I-V curve for positive gate bias is not a typical transistor response, but it does verify that the gate is controlling the current flow in the region between the source and drain. The expected response, if the transistor is still in the “on” mode with 5.0 V gate bias, is that the drain current present at all drain voltages would have the same shape and transition point as the curves for negative gate bias, but with lower current values than are shown with 0.0 V on the gate. If the transistor is in the “off” mode with 5.0 V applied to the gate bias, then the current would not be expected to increase at all. This unexpected response can probably be explained by the fact that the gate current for this device is still higher than the drain and source currents, and so there is substantial gate leakage taking place.

Figure 5.9 plots a typical set of I-V characteristics obtained from the bottom gate BioFET structure with silicon as the gate, 500 nm of SiO_2 as the gate dielectric, gold as the source and drain, and DNA:PEDOT:CTMA as the semiconductor. The current compliance limit is set to 1.0 mA on each terminal. This figure shows that the drain current increases with increasing drain voltage for all gate bias voltages. It also shows that the drain current decreases with increasing gate voltage for any drain voltage. The clustering of current values near zero seen at low drain voltages on this plot is not due to current limiting, but instead is the actual response of the device. This response makes this structure more transistor-like than the characteristics obtained from the structure in Section 5.2. The gate leakage current in this device is still larger than expected for a field effect transistor, and is therefore causing a non-ideal response from the device.

The drain current decreases with increasing gate voltage for these DNA-biopolymer FETs, and gate voltage transitions from negative to positive before the drain current reaches zero. This again indicates that the transistor is a p-channel transistor operating in depletion mode [65].

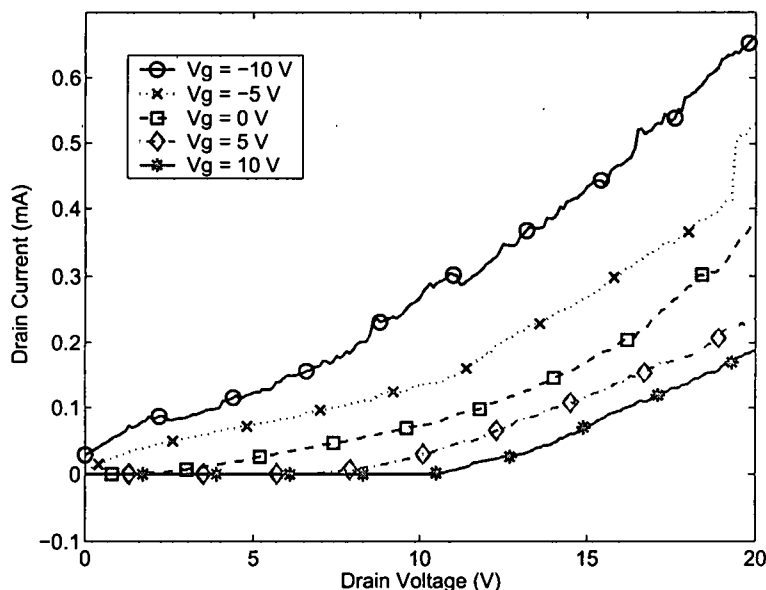
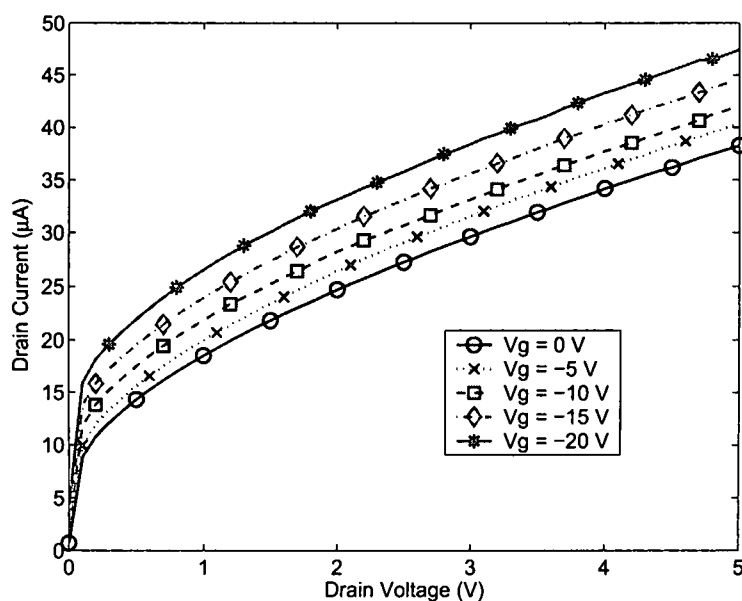
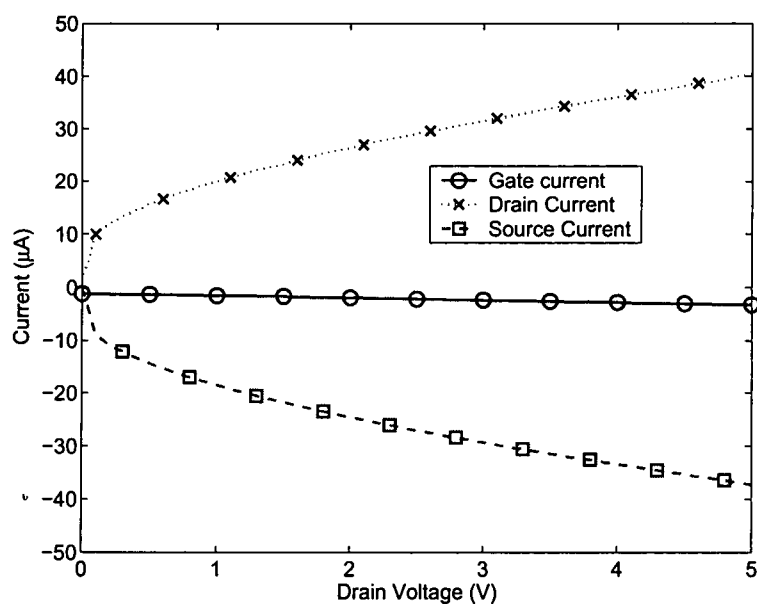


Figure 5.9: Drain current as a function of drain voltage as measured on a bottom gate BioFET on an undoped silicon wafer with an RF sputtered silicon dioxide layer as the gate dielectric.

Figure 5.10a plots the I-V characteristics obtained from another bottom gate BioFET device on an undoped silicon wafer as described at the beginning of Section 5.3. The current compliance limit is set to 0.5 mA on each terminal. This figure shows that for drain voltages from 0.0 to 0.1 V, the drain currents have a steep increase that goes through the origin for all the gate voltages 0.0 to -20.0 V. As the gate voltage increases toward zero, the drain current decreases at positive drain voltages, as one would expect for a depletion mode transistor. These measurements are of particular interest because the gate currents are substantially lower than the source and drain currents for all drain voltages under all gate bias conditions. The gate, source, and drain currents are plotted as a function of drain voltage with -5.0 V on the gate in Figure 5.10b. This figure shows that the gate current is an order of magnitude smaller than the source or drain current for all drain voltages. It also shows that



(a)



(b)

Figure 5.10: (a) Drain current as a function of drain voltage as measured on a bottom gate BioFET on an undoped silicon wafer with a very thin silicon dioxide layer as the gate insulator. (b) Gate, drain and source current is plotted as a function of drain voltage for this device, verifying that the gate current is substantially lower than either the source or drain currents. Note that positive current is current leaving the terminal.

the source and drain currents are always nearly equal in magnitude and opposite in sign, as expected for a transistor when positive current is defined as current leaving the terminal. Both parts of Figure 5.10 are interesting because together they show that if the gate can be successfully isolated from the source and drain, the gate modulates the drain to source current and transistor behavior is observed.

5.3.2 Analysis

The data obtained from the bottom gate BioFETs containing DNA:PEDOT:CTMA show promise for this new material. However, this structure still has high gate currents. These gate currents are potentially due to the presence of mobile charges in the DNA-biopolymers. Drs. Singh and Sarıci, collaborators on this research at Johannes Kepler University of Linz, are investigating the use of blocking layers to control these mobile charges in DNA-based devices.

Analyzing the transistor curves presented above, the linear regions show that the BioFETs fabricated on a very thin layer of SiO₂ have a resistivity that is between 5.4 and 22.9 k Ω . Using a multimeter to measure the resistivity of the device yields resistance values that vary dramatically. This is likely due to poor adhesion of the gold source and drain to the very thin layer of SiO₂, and therefore one can safely assume that the lower resistance values are more accurate. Making this assumption, the measured resistance of these devices is between 16 and 36 k Ω .

The surface resistivity of a similar thin film of DNA:PEDOT:CTMA is measured by the Hall effect to be between 3×10^{12} and 2×10^{13} Ω/sq . Based on the surface resistivity measurements, the DNA:PEDOT:CTMA made with 90 wt% Baytron P to DNA, is too resistive to obtain an accurate and consistent mobility measurement using the Hall effect. Another way to determine the mobility of DNA:PEDOT:CTMA is to apply an oscillating frequency to the drain, and increase that frequency

until the response falls off by 3 dB. However, this cannot be done with the semiconductor characterization system, as it cannot supply an AC voltage. Therefore, the mobility needs to be theoretically determined from the experimentally obtained current and voltages. The drain current equation in the linear region is given by

$$I_D = \mu_{lin} C_i \frac{W}{L} \left[(V_{GS} - V_t) V_{DS} - \frac{1}{2} V_{DS}^2 \right] \quad (5.1)$$

and in the saturation region it is given by

$$I_D = \mu_{sat} C_i \frac{W}{2L} (V_{GS} - V_t)^2 \quad (5.2)$$

where I_D is the drain current, W/L is the ratio of channel width to channel length, μ_{sat} is the mobility in the saturation region, μ_{lin} is the mobility in the linear region, V_{GS} is the gate to source voltage, V_{DS} is the drain to source voltage, C_i is the capacitance per unit area of the insulator, and V_t is the threshold voltage. Complicating these calculations, the mobilities in the linear and saturation regions are not always the same, and often the linear mobility is lower [99]. This means that calculating the mobility in the linear region will only produce a lower bound for the mobility.

For the data reported in this dissertation, the threshold voltage cannot be accurately determined. Therefore the drain current equation in the linear region cannot be used to determine the linear region mobility. Instead, one can use the transconductance, g_m , in the linear region,

$$g_m = \left. \frac{\partial I_D}{\partial V_G} \right|_{V_D} = \frac{W}{L} C_i \mu_{lin} V_D \quad (5.3)$$

where the partial derivative of I_D with respect to V_G is taken for a constant value of V_D , and the variables are as defined above. The mobility of PEDOT:PSS is known to be $10 \text{ cm}^2/(\text{Vs})$ [100]. For the majority of the above devices, the mobility calculated from the slope of the linear portion of the drain current as a function of gate voltage is larger than the mobility of PEDOT:PSS. This is

likely due to the high gate leakage currents found in most of these devices. Therefore, one would expect the mobility for the device with lower gate currents than drain and source currents to have a lower mobility, and it does. Using the procedure described above to calculate the mobility of the device whose data is plotted in Figure 5.10, the linear mobility is calculated to be $0.018 \text{ cm}^2/(\text{Vs})$. This is a reasonable mobility value for an insulator doped with a Baytron P conducting polymer, as it is reasonable to expect the mobility to be lower than the highest mobility material in the complex. Unfortunately, this value is an overestimate of the mobility of DNA:PEDOT:CTMA, because the W/L ratio for the bottom gate devices described in this dissertation is 2.63, and to minimize the effects of fringe currents the W/L ratio should be at least 10.0 [101].

Even without knowing the threshold voltage for the data, the drain current equation in the saturation region, given in Equation 5.2, can be used to calculate the saturation region mobility. Since there are two unknowns, μ_{sat} and V_t , two equations are needed to solve for the saturation mobility. Therefore, the drain currents corresponding to two different gate voltages at the same drain voltage will be used. Figure 5.11 shows how the effective saturation mobility, calculated from the drain currents at zero and negative ten volts applied to the gate, varies with drain voltage. This figure shows that the saturation mobility decreases with increasing drain voltage in the saturation region of operation for the transistor. Therefore, the maximum saturation mobility occurs at the lowest drain voltage in the saturation region. For the transistor reported above to have low gate currents and produce transistor curves, the effective saturation mobility occurs when the drain voltage is 0.2 V. For gate voltages of 0.0 and -10.0 volts, the maximum saturation mobility is calculated to be $0.45 \text{ cm}^2/(\text{Vs})$.

The mobility values obtained using these methods are overestimates due to the low W/L ratio of the device, and therefore the true mobility for this material is still unknown. However, the above

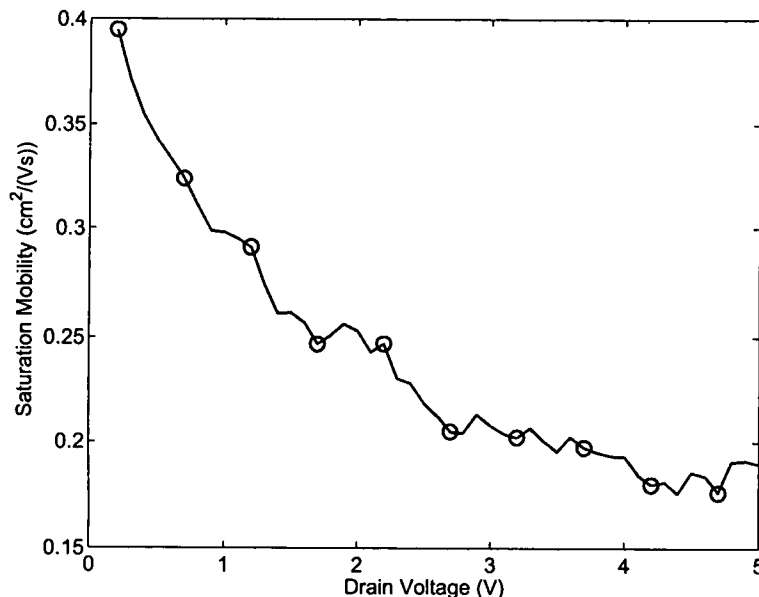


Figure 5.11: Saturation mobility as a function of drain voltage as calculated from the drain current vs. drain voltage data on a bottom gate BioFET with a very thin layer of native silicon dioxide as the gate insulator. The data for this plot is calculated using the drain currents associated with gate voltages of 0 and -10 V, when the drain voltage is 0.2 V, obtained from Figure 5.10.

calculations suggest that the mobility of DNA:PEDOT:CTMA is two orders of magnitude less than the mobility of PEDOT:PSS, the conducting polymer which is combined with DNA to make this biopolymer.

5.4 Summary

This chapter describes the development of the first field effect transistor to demonstrate the use of a DNA-biopolymer as the semiconducting layer. It explores the characteristics of both top gate and bottom gate BioFETs, using DNA-CTMA and DNA:PEDOT:CTMA as potential semiconducting layers in these transistors. Various problems encountered in the development are described

along with some attempted solutions. The first all-DNA BioFET, using DNA:PEDOT:CTMA as the semiconducting layer and DNA-CTMA as the gate insulator, is also fabricated and tested. The biopolymer DNA:PEDOT:CTMA is found to be a more successful semiconductor in transistors than DNA-CTMA alone. Transistors fabricated with DNA:PEDOT:CTMA as the semiconducting layer yield non-linear drain currents as a function of the drain voltage. Even with high gate currents remaining a problem for most of the devices measured, the nonlinear behavior of the DNA-biopolymer is evident and provides promise for the use of DNA-biopolymers in future semiconducting applications.

In the next and final chapter, a summary of the main conclusions from this work, further suggestions for improvement, and potential areas for future work are presented.

CHAPTER VI

CONCLUSIONS AND FUTURE WORK

This chapter summarizes the contributions this dissertation makes to the body of research on DNA-biopolymers. It also explores some areas of future work necessary to further develop and improve field effect transistors using DNA-biopolymers as the semiconducting layer and other electronic applications.

6.1 Contributions

The major contribution of this dissertation is the design, development, fabrication and testing of a field effect transistor using a DNA-biopolymer as the semiconducting layer. DNA is doped with the conducting polymer Baytron P to form DNA:PEDOT:CTMA, which is successfully used as a semiconducting material for the first time. Two transistor structures, a top gate structure with APC as the gate insulator and bottom gate structure with silicon dioxide as the gate insulator, are designed, fabricated, and tested. Both structures are fabricated with the DNA-biopolymer, and the current-voltage characteristics are obtained and presented. For both designs, nonlinear switching behavior is consistently observed. A transistor with low gate current, nonlinear switching, and gate voltage control is designed and measured. The effective mobility of DNA:PEDOT:CTMA in the linear region is around $0.018 \text{ cm}^2/(\text{Vs})$, and in the saturation region it is around $0.45 \text{ cm}^2/(\text{Vs})$. This shows that the effective mobility of DNA:PEDOT:CTMA is two orders of magnitude less than

the published mobility of PEDOT:PSS, the conductive polymer that is combined with DNA to make the new biopolymer.

A second important contribution is the design, analysis and use of a new capacitive test structure for electrical characterization on polymers and biopolymers. A new capacitive test structure is used to characterize the electrical properties of thin films. This capacitive test structure is effective for measuring the S parameters and determining the dielectric properties of polymers and biopolymers. An electrical model for the capacitive test structure is obtained, and after matching the measured S parameters to this electrical model, the dielectric properties of the thin film can be determined. Using capacitive frequency measurements over a range of low frequencies, it is verified that the dielectric properties obtained using the capacitive test structure are the bulk material properties and are not due to transient or interface charges.

Dielectric tunability is observed in the biopolymer thin films. The relative dielectric constant of the DNA-CTMA thin film changes by 52% when the applied bias changes from 0.0 to 20.0 V, which is equivalent to changing the applied field from 0 to 113 kV/cm. The relative dielectric constant of the BSA-PVA thin film at room temperature changes by 44% when the applied bias changes from 0.0 to 20.0 V, which corresponds to changing the electric field from 0 to 86 kV/cm. The tunability of these unoptimized biopolymers at room temperature compare favorably to that of BST, a known material with dielectric tunability, which tunes by 47% when the applied bias changes from 0 to 100 kV/cm. At 100 °C the relative dielectric constant of BSA-PVA tunes by 21% as the bias changes from 0.0 to 20.0 V, which corresponds to changing the electric field from 0 to 86 kV/cm, and by 27% as the bias changes from 5.0 to 10.0 V, corresponding to changing the electric field from 21 to 43 kV/cm. The mechanisms involved in this dielectric tuning are observed and the charge dynamics

are visualized by EFM measurements for the DNA-CTMA thin film at the center of the capacitive test structure.

Another contribution of this dissertation is the determination of the necessary spin parameters and material preparation to obtain thin films of specific thicknesses for various polymer and biopolymer thin films. These parameters include spin speeds and ramp times, along with necessary temperature conditions for the substrate and polymer solution. It is determined that the parameters used to obtain uniform polymer films do not necessarily yield uniform biopolymer films. The biopolymer films require a longer ramp time before spinning at the desired speed, as well as having both the solution and the substrate above room temperature.

6.2 Future Work

This research demonstrates that DNA-biopolymers can be successfully used as semiconducting materials in transistors. However, there are still some issues that need to be worked out to make DNA-biopolymer based field effect transistors production-worthy devices. First, the gate leakage current needs to be consistently reduced. To reduce the gate current, a better insulating layer needs to be identified. An appropriate next step to reduce this current would be to use a better and more uniform silicon dioxide layer. A silicon dioxide layer deposited by dry oxide growth is likely to yield lower gate currents.

Studying the properties of field effect transistors that use DNA-biopolymers as the semiconducting layer is another useful direction for future work. Some of these properties include the pinch-off voltage, the Early voltage, frequency response and the on/off current ratio. Knowing these properties are helpful in understanding the transistor and how it operates.

Obtaining an accurate mobility for the DNA:PEDOT:CTMA biopolymer would also be useful. This measurement can be obtained by applying an AC signal over the DC signal on the drain, and increasing the frequency of the AC signal until the response drops to 3 dB of the original signal. Having a valid mobility measurement is the next step in analyzing this new biopolymer. Now that this biopolymer has been shown to work as a semiconductor, having more detailed knowledge about the specific properties that this biopolymer has will be useful for future device development.

Another potential way of improving the field effect transistor using a DNA-biopolymer as the semiconducting layer would be to vary the amount and type of Baytron P that is added to the DNA. This is currently being studied by researchers in the Materials and Manufacturing Directorate at Wright Patterson Air Force Base. Studying the effects of the ratio of PEDOT to DNA present in DNA:PEDOT:CTMA might provide insight into how the properties are affected by the amount of PEDOT in the complex.

Combining the DNA with various materials that have specific desirable properties, such as high mobility, will provide further insight into how the DNA-biopolymers are affected by the properties of the materials that are combined with the DNA. While different materials are likely to affect the properties of DNA-biopolymers in various ways, an introductory material study on how the properties of DNA-biopolymers are affected by the addition of materials is needed to determine which properties of the DNA-biopolymers are the easiest to influence.

This dissertation also successfully showed the use of a new capacitive test structure to determine the dielectric properties of thin films. While this work produced some interesting results, there are still many variations that should be characterized. First, one should study how the dielectric properties of these polymer and biopolymer materials vary with film thickness. This will give

useful insight into how the thickness of thin films affects their properties, especially for the DNA-biopolymers which are made from the long DNA backbone. Second, determining the relationship between the molecular weight of the DNA used in the DNA-biopolymer and the dielectric properties of that biopolymer is important. Understanding the effect on the dielectric properties of using various molecular weights of DNA in the DNA-CTMA biopolymer will help understand where DNA-CTMA can be utilized most effectively in electronic and electro-optic applications. This understanding will also help determine the optimal molecular weight of DNA to use in the biopolymer for various applications. Third, studying the dielectric properties of various DNA-biopolymers and the materials added to the DNA in these biopolymers, such as DNA:PEDOT:CTMA and Baytron P, will give useful insight into how the dielectric properties of the DNA-biopolymers can be influenced by the materials added to the DNA in these biopolymers.

BIBLIOGRAPHY

- [1] D. D. Ebbing, *General chemistry*, 5th ed. Boston: Houghton Mifflin, 1996.
- [2] R. Carrillo-Ramirez and R. W. Jackson, "A highly integrated millimeter-wave active antenna array using BCB and silicon substrate," *IEEE Transactions on Microwave Theory and Techniques*, vol. 52, no. 6, pp. 1648–1653, 2004.
- [3] P. E. Garrou, W. B. Rogers, D. M. Scheck, A. J. G. Strandjord, Y. Ida, and K. Ohba, "Stress-buffer and passivation processes for Si and GaAs IC's and passive components using photosensitive BCB: process technology and reliability data," *IEEE Transactions on Advanced Packaging*, vol. 22, no. 3, pp. 487–498, 1999.
- [4] X. Huo, K. J. Chen, and P. C. H. Chan, "Silicon-based high-Q inductors incorporating electroplated copper and low-K BCB dielectric," *IEEE Electron Device Letters*, vol. 23, no. 9, pp. 520–522, 2002.
- [5] S. K. Park, Y. H. Kim, J. I. Han, D. G. Moon, and W. K. Kim, "High-performance polymer TFTs printed on a plastic substrate," *IEEE Transactions on Electron Devices*, vol. 49, no. 11, pp. 2008–2015, 2002.
- [6] Y. Kato, S. Iba, R. Teramoto, T. Sekitani, T. Someya, H. Kawaguchi, and T. Sakurai, "High mobility of pentacene field-effect transistors with polyimide gate dielectric layers," *Applied Physics Letters*, vol. 84, no. 19, pp. 3789–3791, 2004.
- [7] K. N. N. Unni, S. Dabos-Seignon, and J.-M. Nunzi, "Improved performance of pentacene field-effect transistors using a polyimide gate dielectric layer," *Journal of Physics D: Applied Physics*, no. 8, pp. 1148–1151, 2005.
- [8] J. Puigdollers, C. Voz, I. Martin, M. Vetter, A. Orpella, and R. Alcubilla, "Electrical characterization of pentacene thin-film transistors with polymeric gate dielectric," *Synthetic Metals*, vol. 146, no. 3, pp. 355–358, 2004.
- [9] A. Kuntman and H. Kuntman, "A study on dielectric properties of a new polyimide film suitable for interlayer dielectric material in microelectronics applications," *Microelectronics Journal*, vol. 31, no. 8, pp. 629–634, 2000.

- [10] B. C. Auman, D. P. Higley, K. V. Scherer Jr., E. F. McCord, and W. H. Shaw Jr., "Synthesis of a new fluoroalkylated diamine, 5-[1H,1 H-2bis(trifluoromethyl)- heptafluoropentyl]-1,3-phenylenediamine, and polyimides prepared therefrom," *Polymer*, vol. 36, no. 3, pp. 651–656, 1995.
- [11] H. A. Reed, C. E. White, V. Rao, S. A. B. Allen, C. L. Henderson, and P. A. Kohl, "Fabrication of microchannels using polycarbonates as sacrificial materials," *Journal of Micromechanics and Microengineering*, vol. 11, no. 6, p. 733, 2001.
- [12] E. M. Heckman, P. P. Yaney, J. G. Grote, F. K. Hopkins, and M. M. Tomczak, "Development of an all-DNA-surfactant electro-optic modulator," in *Organic Photonic Materials and Devices VIII*, vol. 6117. San Jose, CA, USA: SPIE, 2006, pp. 61 170K–7.
- [13] J. A. Hagen, W. X. Li, J. G. Grote, and A. J. Steckl, "Red/blue electroluminescence from europium-doped organic light emitting diodes," in *Organic Photonic Materials and Devices VIII*, vol. 6117. San Jose, CA, USA: SPIE, 2006, pp. 61 170O–5.
- [14] J. A. Hagen, W. Li, A. J. Steckl, and J. G. Grote, "Enhanced emission efficiency in organic light-emitting diodes using deoxyribonucleic acid complex as an electron blocking layer," *Applied Physics Letters*, vol. 88, no. 17, p. 171109, 2006.
- [15] B. Singh, N. S. Sariciftci, J. G. Grote, and F. K. Hopkins, "Bio-organic-semiconductor-field-effect-transistor based on deoxyribonucleic acid gate dielectric," *Journal of Applied Physics*, vol. 100, no. 2, pp. 024 514–4, 2006.
- [16] J. G. Grote, E. M. Heckman, J. A. Hagen, P. P. Yaney, D. E. Diggs, G. Subramanyam, R. L. Nelson, J. S. Zetts, D. Y. Zang, B. Singh, N. S. Sariciftci, and F. K. Hopkins, "DNA: new class of polymer," in *Organic Photonic Materials and Devices VIII*, vol. 6117. San Jose, CA, USA: SPIE, 2006, pp. 61 170J–6.
- [17] J. G. Grote, E. Heckman, J. A. Hagen, P. P. Yaney, G. Subramanyam, S. J. Clarson, D. E. Diggs, R. L. Nelson, J. S. Zetts, F. K. Hopkins, and N. Ogata, "Deoxyribonucleic acid (DNA) based optical materials," in *Optical Materials in Defense Systems Technology*, vol. 5621. London, United Kingdom: International Society for Optical Engineering, Bellingham, WA 98227-0010, United States, 2004, pp. 16–22.
- [18] P. T. Henderson, D. Jones, G. Hampikian, Y. Kan, and G. B. Schuster, "Long-distance charge transport in duplex DNA: The phonon-assisted polaron-like hopping mechanism," *PNAS*, vol. 96, no. 15, pp. 8353–8358, 1999.
- [19] G. Zhang, H. Takahashi, L. Wang, J. Yoshida, S. Kobayashi, S. Horinouchi, and N. Ogata, "Nonlinear optical materials derived from biopolymer (DNA)-surfactant azo dye complex," in *Materials and Devices for Optical and Wireless Communications*, vol. 4905. Shanghai, China: SPIE, 2002, pp. 375–380.

- [20] E. M. Heckman, J. G. Grote, F. K. Hopkins, and P. P. Yaney, "Performance of an electro-optic waveguide modulator fabricated using a deoxyribonucleic-acid-based biopolymer," *Applied Physics Letters*, vol. 89, no. 18, pp. 181 116–3, 2006.
- [21] E. L. Gelamo, C. H. T. P. Silva, H. Imasato, and M. Tabak, "Interaction of bovine (BSA) and human (HSA) serum albumins with ionic surfactants: spectroscopy and modelling," *Biochimica et Biophysica Acta (BBA) - Protein Structure and Molecular Enzymology*, vol. 1594, no. 1, pp. 84–99, 2002.
- [22] S. Kavlak and A. Gner, "Intermolecular interactions between bovine serum albumin and certain water-soluble polymers at various temperatures," *Journal of Applied Polymer Science*, vol. 100, no. 2, pp. 1554–1560, 2006.
- [23] P. A. Vazquez-Landaverde, E. M. Sanchez, and J. A. Huerta-Ruelas, "Optical techniques coupled to ohmic heating to study heat-induced changes in biological systems," in *Sixth Symposium Optics in Industry*, vol. 6422. Monterrey, Mexico: SPIE, 2007, pp. 64 220F–7.
- [24] C. M. Bartsch, G. Subramanyam, J. Grote, F. K. Hopkins, L. L. Brott, and R. R. Naik, "A new capacitive test structure for microwave characterization of biopolymers," *Microwave and Optical Technology Letters*, vol. 49, no. 6, pp. 1261–1265, 2007.
- [25] K.-K. Lee and B. C. Kim, "Benzocyclobutene (BCB) based spiral inductor for wireless application," in *MEMS/MOEMS Components and Their Applications II*, vol. 5717. SPIE, 2005, pp. 66–70.
- [26] T. Hwang, D. Popa, J. Sin, H. E. Stephanou, and E. M. Leonard, "BCB wafer bonding for microfluidics," in *Micromachining and Microfabrication Process Technology IX*, vol. 5342. San Jose, CA, USA: SPIE, 2004, pp. 182–191.
- [27] K. Nishikawa, S. Sugitani, K. Kamogawa, T. Tokumitsu, I. Toyoda, and M. Tanaka, "A compact V-band 3-D MMIC single-chip down-converter using photosensitive BCB dielectric film," *IEEE Transactions on Microwave Theory and Techniques*, vol. 47, no. 12, pp. 2512–2518, 1999.
- [28] Y.-S. Choi, J.-S. Park, H.-D. Park, Y.-H. Song, J.-S. Jung, and S.-G. Kang, "Effects of temperatures on microstructures and bonding strengths of Si-Si bonding using bisbenzocyclobutene," *Sensors and Actuators A: Physical*, vol. 108, no. 1-3, pp. 201–205, 2003.
- [29] S. Agan, F. Ay, A. Kocabas, and A. Aydinli, "Stress effects in prism coupling measurements of thin polymer films," *Applied Physics A: Materials Science & Processing*, vol. 80, no. 2, pp. 341–345, 2005.
- [30] K.-I. Kim, J.-M. Kim, J.-M. Kim, G.-C. Hwang, C.-W. Baek, and Y.-K. Kim, "Packaging for RF MEMS devices using LTCC substrate and BCB adhesive layer," *Journal of Micromechanics and Microengineering*, vol. 16, no. 1, pp. 150–156, 2006.

- [31] K. Lee, J. He, R. Clement, S. Massia, and B. Kim, "Biocompatible benzocyclobutene (BCB)-based neural implants with micro-fluidic channel," *Biosensors and Bioelectronics*, vol. 20, no. 2, pp. 404–407, 2004.
- [32] H. Deligoz, S. Ozgumus, T. Yalcinyuva, S. Yildirim, D. Deger, and K. Ulutas, "A novel cross-linked polyimide film: synthesis and dielectric properties," *Polymer*, vol. 46, no. 11, pp. 3720–3729, 2005.
- [33] S.-J. Park, K.-S. Cho, and S.-H. Kim, "A study on dielectric characteristics of fluorinated polyimide thin film," *Journal of Colloid and Interface Science*, vol. 272, no. 2, pp. 384–390, 2004.
- [34] A. Darwish, A. Ezzeddine, H. C. Huang, and M. Mah, "Properties of the embedded transmission line (ETL)-an offset stripline with two dielectrics," *IEEE Microwave and Guided Wave Letters*, vol. 9, no. 6, pp. 224–226, 1999.
- [35] B. Chandar Shekar, V. Veeravazhuthi, S. Sakthivel, D. Mangalaraj, and S. K. Narayandass, "Growth, structure, dielectric and AC conduction properties of solution grown PVA films," *Thin Solid Films*, vol. 348, no. 1-2, pp. 122–129, 1999.
- [36] C. V. Subba Reddy, X. Han, Q.-Y. Zhu, L.-Q. Mai, and W. Chen, "Dielectric spectroscopy studies on (PVP + PVA) polyblend film," *Microelectronic Engineering*, vol. 83, no. 2, pp. 281–285, 2006.
- [37] H. P. de Oliveira, M. V. B. dos Santos, C. G. dos Santos, and C. P. de Melo, "Electrical properties of PVA/PPY blends," *Synthetic Metals*, vol. 135-136, pp. 447–448, 2003.
- [38] H. P. de Oliveira, M. V. B. dos Santos, C. G. dos Santos, and C. P. de Melo, "Preparation and electrical and dielectric characterization of PVA/PPY blends," *Materials Characterization*, vol. 50, no. 2-3, pp. 223–226, 2003.
- [39] Q. Feng, Z. Dang, N. Li, and X. Cao, "Preparation and dielectric property of Ag-PVA nanocomposite," *Materials Science and Engineering B*, vol. 99, no. 1-3, pp. 325–328, 2003.
- [40] M. A. Ahmed and M. S. Abo-Ellil, "Effect of dopant concentration on the electrical properties of polyvinyl alcohol (PVA)," *Journal of Materials Science: Materials in Electronics*, vol. 9, no. 5, pp. 391–395, 1998.
- [41] L. L. Brott, S. M. Rozenzhak, R. R. Naik, S. R. Davidson, R. E. Perrin, and M. O. Stone, "A poly(vinyl alcohol)/carbon-black composite film: A platform for biological macromolecule incorporation," *Advanced Materials*, vol. 16, no. 7, pp. 592–596, 2004.
- [42] J. Mijovic, J. W. Sy, and T. K. Kwei, "Reorientational dynamics of dipoles in poly(vinylidene fluoride)/poly(methyl methacrylate) (PVDF/PMMA) blends by dielectric spectroscopy," *Macromolecules*, vol. 30, no. 10, pp. 3042–3050, 1997.

- [43] S. Bistac and J. Schultz, "Study of solution-cast films of PMMA by dielectric spectroscopy: Influence of the nature of the solvent on $[\alpha]$ and $[\beta]$ relaxations," *International Journal of Adhesion and Adhesives*, vol. 17, no. 3, pp. 197–201, 1997.
- [44] S. Bistac and J. Schultz, "Solvent retention in solution-cast films of PMMA: study by dielectric spectroscopy," *Progress in Organic Coatings*, vol. 31, no. 4, pp. 347–350, 1997.
- [45] K. Miyairi, "The frequency dependent dielectric breakdown in some thin polymers," in *7th International Conference on Properties and Applications of Dielectric Materials*, vol. 3, Nagoya, Japan, 2003, pp. 949–952 vol.3.
- [46] V. Svorcik, T. Podgrabinski, J. Nahlik, V. Rybka, and V. Hnatowicz, "Dielectric properties of doped polymethylmethacrylate," *Materials Letters*, vol. 59, no. 2-3, pp. 341–344, 2005.
- [47] W. Zheng and S.-C. Wong, "Electrical conductivity and dielectric properties of PMMA/expanded graphite composites," *Composites Science and Technology*, vol. 63, no. 2, pp. 225–235, 2003.
- [48] H. M. Zidan and M. Abu-Elnader, "Structural and optical properties of pure PMMA and metal chloride-doped PMMA films," *Physica B: Condensed Matter*, vol. 355, no. 1-4, pp. 308–317, 2005.
- [49] M. El-Shabasy and A. S. Riad, "Dielectric behaviour of polycarbonate," *Physica B: Condensed Matter*, vol. 222, no. 1-3, pp. 153–159, 1996.
- [50] L. M. Hayden, A. M. Sinyukov, M. R. Leahy, J. French, P. Lindahl, W. N. Herman, R. J. Twieg, and M. He, "New materials for optical rectification and electrooptic sampling of ultrashort pulses in the terahertz regime," *Journal of Polymer Science Part B: Polymer Physics*, vol. 41, no. 21, pp. 2492–2500, 2003.
- [51] S. Santos, A. Cedeo, and C. Gmez, "DC conductivity and dielectric response in amorphous polycarbonate of Bisphenol-A," *Polymer Engineering & Science*, vol. 39, no. 9, pp. 1752–1756, 1999.
- [52] S. Ermer, S. M. Lovejoy, P. V. Bedworth, D. S. Leung, H. B. Warren, J. A. Epstein, D. G. Girton, L. S. Dries, R. E. Taylor, R. R. Barto Jr, W. Eades, T. E. Van Eck, A. S. Moss, and W. W. Anderson, "Low-voltage electro-optic modulation using amorphous polycarbonate host material," *Advanced Functional Materials*, vol. 12, no. 9, pp. 605–610, 2002.
- [53] E. M. Heckman, J. A. Hagen, P. P. Yaney, J. G. Grote, and F. K. Hopkins, "Processing techniques for DNA: a biopolymer for photonics applications," *Applied Physics Letters*, vol. 87, no. 21, p. 211115, 2005.
- [54] L. Wang, J. Yoshida, N. Ogata, S. Sasaki, and T. Kajiyama, "Self-assembled supramolecular films derived from marine deoxyribonucleic acid (DNA)-cationic surfactant complexes:

- Large-scale preparation and optical and thermal properties," *Chem. Mater.*, vol. 13, no. 4, pp. 1273–1281, 2001.
- [55] P. P. Yaney, E. M. Heckman, A. Davis, J. A. Hagen, C. M. Bartsch, G. Subramanyam, J. G. Grote, and F. K. Hopkins, "Characterization of NLO polymer materials for optical waveguide structures," in *Organic Photonic Materials and Devices VIII*, vol. 6117. San Jose, CA, USA: SPIE, 2006, pp. 61 170W–14.
- [56] P. Queffelec, P. Gelin, J. Gieraltowski, and J. Loaec, "A microstrip device for the broad band simultaneous measurement of complex permeability and permittivity," *Magnetics, IEEE Transactions on*, vol. 30, no. 2, pp. 224–231, 1994.
- [57] C. Brosseau, P. Queffelec, and P. Talbot, "Microwave characterization of filled polymers," *Journal of Applied Physics*, vol. 89, no. 8, pp. 4532–4540, 2001.
- [58] W. B. Weir, "Automatic measurement of complex dielectric constant and permeability at microwave frequencies," *Proceedings of the IEEE*, vol. 62, no. 1, pp. 33–36, 1974.
- [59] M. D. Janezic, D. F. Williams, V. Blaschke, A. Karamcheti, and C. Chi Shih, "Permittivity characterization of low-k thin films from transmission-line measurements," *Microwave Theory and Techniques, IEEE Transactions on*, vol. 51, no. 1, pp. 132–136, 2003.
- [60] G. Subramanyam, E. Heckman, J. Grote, and F. Hopkins, "Microwave dielectric properties of DNA based polymers between 10 and 30 GHz," *IEEE Microwave and Wireless Components Letters*, vol. 15, no. 4, pp. 232–234, 2005.
- [61] D. Ghosh, B. Laughlin, J. Nath, A. I. Kingon, M. B. Steer, and J. P. Maria, "Tunable high-quality-factor interdigitated (Ba, Sr)TiO₃ capacitors fabricated on low-cost substrates with copper metallization," *Thin Solid Films*, vol. 496, no. 2, pp. 669–673, 2006.
- [62] S. W. Kirchoefer, J. M. Pond, A. C. Carter, W. Chang, K. K. Agarwal, J. S. Horwitz, and D. B. Chrisey, "Microwave properties of Sr_{0.5}Ba_{0.5}TiO₃ thin-film interdigitated capacitors," *Microwave and Optical Technology Letters*, vol. 18, no. 3, pp. 168–171, 1998.
- [63] J.-H. Koh and A. Grishin, "Ag(Ta, Nb)O₃ thin-film low-loss variable interdigital capacitors," *Applied Physics Letters*, vol. 79, no. 14, pp. 2234–2236, 2001.
- [64] J. Singh, *Semiconductor devices: basic principles*. New York: Wiley, 2001.
- [65] A. S. Sedra and K. C. Smith, *Microelectronic circuits*, 4th ed. New York: Oxford University Press, 1998.
- [66] T. Yamamoto, T. Yasuda, Y. Sakai, and S. Aramaki, "Ambipolar field-effect transistor (FET) and redox characteristics of a π -conjugated thiophene/1,3,4-thiadiazole CT-type copolymer," *Macromolecular Rapid Communications*, vol. 26, no. 15, pp. 1214–1217, 2005.

- [67] M. J. Deen, M. H. Kazemeini, Y. M. Haddara, Y. Jianfei, G. Vamvounis, S. Holdcroft, and W. Woods, "Electrical characterization of polymer-based FETs fabricated by spin-coating poly(3-alkylthiophene)s," *Electron Devices, IEEE Transactions on*, vol. 51, no. 11, pp. 1892–1901, 2004.
- [68] S. Uemura, M. Yoshida, S. Hoshino, T. Kodzasa, and T. Kamata, "Investigation for surface modification of polymer as an insulator layer of organic FET," *Thin Solid Films*, vol. 438–439, pp. 378–381, 2003.
- [69] G. W. Kang, K. M. Park, J. H. Song, C. H. Lee, and D. H. Hwang, "The electrical characteristics of pentacene-based organic field-effect transistors with polymer gate insulators," *Current Applied Physics*, vol. 5, no. 4, pp. 297–301, 2005.
- [70] S. Ashizawa, Y. Shinohara, H. Shindo, Y. Watanabe, and H. Okuzaki, "Polymer FET with a conducting channel," *Synthetic Metals*, vol. 153, no. 1–3, pp. 41–44, 2005.
- [71] J. S. Swensen, C. Soci, and A. J. Heeger, "Light emission from an ambipolar semiconducting polymer field-effect transistor," *Applied Physics Letters*, vol. 87, no. 25, pp. 253 511–3, 2005.
- [72] T. Sakanoue, E. Fujiwara, R. Yamada, and H. Tada, "Visible light emission from polymer-based field-effect transistors," *Applied Physics Letters*, vol. 84, no. 16, pp. 3037–3039, 2004.
- [73] H. Rost, J. Ficker, J. S. Alonso, L. Leenders, and I. McCulloch, "Air-stable all-polymer field-effect transistors with organic electrodes," *Synthetic Metals*, vol. 145, no. 1, pp. 83–85, 2004.
- [74] T. G. Backlund, H. G. O. Sandberg, R. Osterbacka, H. Stubb, T. Makela, and S. Jussila, "Towards all-polymer field-effect transistors with solution processable materials," *Synthetic Metals*, vol. 148, no. 1, pp. 87–91, 2005.
- [75] M. Yoshida, S. Uemura, T. Kodzasa, T. Kamata, M. Matsuzawa, and T. Kawai, "Surface potential control of an insulator layer for the high performance organic FET," *Synthetic Metals*, vol. 137, no. 1–3, pp. 967–968, 2003.
- [76] L. Edman, J. Swensen, D. Moses, and A. J. Heeger, "Toward improved and tunable polymer field-effect transistors," *Applied Physics Letters*, vol. 84, no. 19, pp. 3744–3746, 2004.
- [77] T. V. Krishna, J. R. Jessing, D. D. Russell, J. Scaggs, L. R. Warner, and J. A. Hartman, "Modeling and design of polythiophene gate electrode chemFETs for environmental pollutant sensing," 2003, pp. 271–274.
- [78] N. Kazanskaya, A. Kukhtin, M. Manenkova, N. Reshetilov, L. Yarysheva, O. Arzhakova, A. Volynskii, and N. Bakeyev, "FET-based sensors with robust photosensitive polymer membranes for detection of ammonium ions and urea," *Biosensors and Bioelectronics*, vol. 11, no. 3, pp. 253–261, 1996.

- [79] S. Dutta and K. S. Narayan, "Gate-voltage control of optically- induced charges and memory effects in polymer field-effect transistors," *Advanced Materials*, vol. 16, no. 23-24, pp. 2151–2155, 2004.
- [80] M. J. Deen and M. H. Kazemeini, "Photosensitive polymer thin-film FETs based on poly(3-octylthiophene)," *Proceedings of the IEEE*, vol. 93, no. 7, pp. 1312–1320, 2005.
- [81] C. Gao, X. Zhu, J.-W. Choi, and C. H. Ahn, "A disposable polymer field effect transistor (FET) for pH measurement," in *12th International Conference on Solid State Sensors, Actuators and Microsystems*, vol. 2, Boston, 2003, pp. 1172–1175 vol.2.
- [82] J. A. Covington, J. W. Gardner, and J. V. Hatfield, "Conducting polymer FET devices for vapor sensing," in *Smart Structures and Materials 1999: Smart Electronics and MEMS*, vol. 3673. Newport Beach, CA, USA: SPIE, 1999, pp. 296–307.
- [83] S.-M. Lee, S.-J. Uhm, J.-I. Bang, K.-D. Song, B.-S. Joo, Y.-S. Lee, and D.-D. Lee, "A field effect transistor type gas sensor based on polyaniline," in *The 13th International Conference on Solid-State Sensors, Actuators and Microsystems (Transducers '05)*. Seoul, Korea: IEEE, 2005, pp. 1935–1938.
- [84] J. A. Covington, J. W. Gardner, D. Briand, and N. F. de Rooij, "A polymer gate FET sensor array for detecting organic vapours," *Sensors and Actuators B: Chemical*, vol. 77, no. 1-2, pp. 155–162, 2001.
- [85] G. Zhang, L. Wang, J. Yoshida, and N. Ogata, "Optical and optoelectronic materials derived from biopolymer deoxyribonucleic acid (DNA)," in *Optoelectronics, Materials, and Devices for Communications*, vol. 4580. Beijing, China: SPIE, 2001, pp. 337–346.
- [86] J. A. Hagen, J. G. Grote, K. M. Singh, R. R. Naik, T. B. Singh, and N. S. Sariciftci, "Deoxyribonucleic acid biotronics," in *Organic Photonic Materials and Devices IX*, vol. 6470. San Jose, CA, USA: SPIE, 2007, pp. 64 700B–4.
- [87] J. Sambrook, *Molecular cloning: a laboratory manual*, 3rd ed. Cold Spring Harbor, N.Y.: Cold Spring Harbor Laboratory Press, 2001, vol. 1.
- [88] S. Wolf and R. N. Tauber, *Silicon processing for the VLSI era*, 2nd ed. Sunset Beach, Calif.: Lattice Press, 2000, vol. 1.
- [89] E. M. Heckman, "The development of an all-DNA-based electro-optic waveguide modulator," Ph.D. dissertation, University of Dayton, 2006.
- [90] J. A. Hagen, W. X. Li, H. Spaeth, J. G. Grote, and A. J. Steckl, "Molecular beam deposition of DNA nanometer films," *Nano Letters*, vol. 7, no. 1, pp. 133–137, 2007.
- [91] D. M. Pozar, *Microwave engineering*, 2nd ed. New York: Wiley, 1998.

- [92] F. Ahamed and G. Subramanyam, "Design of a Si MMIC compatible ferroelectric varactor shunt switch for microwave applications," *Proceedings of the IEEE International Symposium on Applications of Ferroelectrics*, pp. 285–288, 2004.
- [93] F. Purroy and L. Pradell, "New theoretical analysis of the LRRM calibration technique for vector network analyzers," *Instrumentation and Measurement, IEEE Transactions on*, vol. 50, no. 5, pp. 1307–1314, 2001.
- [94] P. Russell, D. Batchelor, and J. T. Thornton, "SEM and AFM: Complementary techniques for high resolution surface investigations," Veeco Instruments Inc., Application Notes AN46, Rev A1, 2004.
- [95] C. Prater, P. Maivald, K. Kjoller, and M. Heaton, "Tappingmode imaging applications and technology," Veeco Instruments, Inc., Application Notes AN04, Rev. A1, 2004.
- [96] F. Serry, K. Kjoller, J. Thornton, R. Tench, and D. Cook, "Electric force microscopy, surface potential imaging, and surface electric modification with the atomic force microscope," Veeco Instruments, Inc., Application Notes AN27, Rev A1, June 1 2004.
- [97] K. Babcock and C. Prater, "Phase imaging: Beyond topography," Veeco Instruments, Inc., Application Notes AN11, Rev. A1, 2004.
- [98] J. N. Haddock, X. Zhang, S. Zheng, Q. Zhang, S. R. Marder, and B. Kippelen, "A comprehensive study of short channel effects in organic field-effect transistors," *Organic Electronics*, vol. 7, pp. 45–54, 2006.
- [99] C. R. Newman, C. D. Frisbie, D. A. daSilvaFilho, J. L. Bredas, P. C. Ewbank, and K. R. Mann, "Introduction to organic thin film transistors and design of n-channel organic semiconductors," *Chem. Mater.*, vol. 16, no. 23, pp. 4436–4451, 2004.
- [100] J. H. Park, O. Waldmann, F. C. Hsu, N. R. Chiou, V. N. Prigodin, Y. Kim, and J. A. Epstein, "Fabrication and IV characteristics of PEDOT-PSS based field effect devices and their applications to electric circuits," in *American Physical Society Annual Meeting*. Austin, Texas: American Physical Society, 2003.
- [101] C. D. Dimitrakopoulos and P. R. L. Malenfant, "Organic thin film transistors for large area electronics," *Advanced Materials*, vol. 14, no. 2, pp. 99–117, 2002.

VITA

- November 3, 1978 Born in Tonawanda, NY to Cynthia (Saj) and John E. Harder Jr.
- 2000 Graduated *summa cum laude* with B.S. in Electrical Engineering from the State University of New York at Buffalo in Buffalo, NY
- 2002 Graduated with M.S.E. in Electrical Engineering from the University of Michigan in Ann Arbor, MI
- July 12, 2003 Married Mark A. Bartsch, son of Judy (Herbst) and Thomas Bartsch
- 2003-2004 Faculty at ITT Technical Institute in Canton, MI
- 2007 Graduated with Ph.D. in Electrical Engineering from the University of Dayton in Dayton, OH

AWARDS

- 2007 First Place - IEEE Dayton Section Graduate Student Paper Competition
- 2005-2007 Tuition plus Research Assistantship from Dayton Area Graduate Studies Institute (DAGSI)
- 2001-2003, 2004-2005 National Science Foundation Graduate Student Fellow
- 2000 Honorable Mention - Eta Kappa Nu's Outstanding Electrical Engineering Student Award

PUBLICATIONS

Referred Journal Articles

C. M. Bartsch, G. Subramanyam, J. Grote, F. K. Hopkins, L. L. Brott, and R. R. Naik, "A New Capacitive Test Structure for Microwave Characterization of Biopolymers," *Microwave and Optical Technology Letters*, vol. 49, pp. 1261-1265, 2007.

G. Subramanyam, C. M. Bartsch, J. Grote, R. R. Naik, L. L. Brott, M. Stone, A. Campbell, "Experimental Verification of Large Dielectric Tunability in DNA-based Biopolymers Over a Wide Frequency Range," submitted to *IEEE Transactions on Nanobioscience*.

Conference Proceedings

C. M. Bartsch, G. Subramanyam, J. G. Grote, F. K. Hopkins, L. L. Brott, and R. R. Naik, "Dielectric and Electrical Transport Properties of Biopolymers," in *Organic Photonic Materials and Devices IX*, vol. 6470, San Jose, CA, USA:SPIE, 2007, pp. 64700C-8.

C. M. Bartsch, G. Subramanyam, J. G. Grote, F. K. Hopkins, L. L. Brott, and R. R. Naik, "Microwave Dielectric Properties of Biopolymers," in *Optical Materials in Defense Systems Technology III*, vol. 6401, Stockholm, Sweden:SPIE, 2006, pp. 640107-6.

P. P. Yaney, E. M. Heckman, A. Davis, J. A. Hagen, C. M. Bartsch, G. Subramanyam, J. G. Grote, and F. K. Hopkins, "Characterization of Polymer Materials for Optical Waveguide Structures," in *Organic Photonic Materials and Devices VIII*, vol. 6117, San Jose, CA, USA: SPIE, 2006.

P. M. Sweeney, C. M. Harder, M. C. Cheung, A. N. Cartwright, F. H. Long, M. E. Aumer, S. F. LeBoeuf, and S. M. Bedair, "Optimizing Light Emission from Nitride Quantum Wells," in *GaAs MANTECH Conference*, Las Vegas, NV (2001).

Conference Presentations

P. P. Yaney, C. M. Bartsch, E. M. Heckman, J. G. Grote, "Studies of resistivity, poling, and spectra of DNA," presented at the International Biotronics Workshop, Big Island, Hawaii, USA, 2007.

C. M. Bartsch, G. Subramanyam, J. G. Grote, F. K. Hopkins, L. L. Brott, R. R. Naik, and H. S. Axtell, "Microwave Dielectric Properties of Biopolymers," presented at Great Lakes Photonics Symposium, SPIE, Dayton, OH, USA 2006.

P. M. Sweeney, C. M. Harder, M. C. Cheung, A. N. Cartwright, "Carrier Dynamics in III-N Quantum Well Structures," Paper NE04-12, presented at Opto Northeast and Imaging 2001, Northeast Regional Meeting on Optoelectronics, Photonics and Imaging, Rochester, NY, USA, 2001.

R702033820